MATERIALS CHEMISTRY
FRONTIERS

REVIEW

Cite this: *Mater. Chem. Front.*, 2018, **2**, 235

Multifunctional second barrier layers for lithium–sulfur batteries

Wei Fan, [a] Longsheng Zhang [b] and Tianxi Liu *[ab]

Lithium–sulfur (Li–S) batteries have become one of the most promising candidates for next-generation energy storage devices due to their high theoretical energy density and cost effectiveness. However, the detrimental shuttle effect of lithium polysulfides during cycling and their deposition on the lithium anode have severely restricted the practical applications of Li–S batteries. Various efforts have been explored in the past few years to hinder the undesirable diffusion and shuttling of lithium polysulfides. The introduction of a second barrier layer has been demonstrated to be a successful approach to restrict the migration of polysulfides and fabricate high-performance Li–S batteries with enhanced cycling and rate performance. A comprehensive review of recent efforts regarding second barrier layers applied in Li–S batteries, either being an individual interlayer, a thin coating on the separator, or an integrated structure, is presented and discussed. Individual interlayers made by porous carbon, carbon/metal compounds and conductive polymers between the separator and the sulfur cathode as well as functionalized polyolefin and non-polyolefin based separators have been proposed. In addition, some advanced examples of interlayers with novel sandwiched/integrated configurations for Li–S batteries, which can not only enable a suppressed shuttle effect but also achieve enhanced energy density, are also reviewed.

Received 2nd September 2017,
Accepted 13th November 2017

DOI: 10.1039/c7qm00405b

rsc.li/frontiers-materials

1 Introduction

The ever-increasing demand for economic and efficient energy storage technologies has triggered the continuous exploration of advanced battery systems.[1–10] Lithium–sulfur (Li–S) batteries with high theoretical energy density (2600 W h kg^{-1}) and high specific capacity (1675 mA h g^{-1}), have become one of the most promising candidates for next-generation energy storage

[a] *State Key Laboratory for Modification of Chemical Fibers and Polymer Materials, College of Materials Science and Engineering, Donghua University, 2999 North Renmin Road, Shanghai 201620, P. R. China. E-mail: txliu@fudan.edu.cn, txliu@dhu.edu.cn*

[b] *State Key Laboratory of Molecular Engineering of Polymers, Department of Macromolecular Science, Fudan University, Shanghai, 200433, P. R. China*

Wei Fan

Wei Fan received her BE in composite materials and engineering at East China University of Science and Technology in 2010, and her PhD in macromolecular chemistry and physics at Fudan University in 2015. As an exchange student, she visited the Singapore Institute of Materials Research and Engineering in 2012, and then School of Chemical and Biomedical Engineering at Singapore Nanyang Technological University in 2013. She is currently an assistant professor in the Department of Materials Science and Engineering at Donghua University. Her research focuses on low-dimensional carbon nanomaterials, aerogel hybrid materials and polymer nanocomposites.

Longsheng Zhang

Longsheng Zhang received his BE at South China University of Technology in 2013, and MS at Fudan University in 2016. He is currently a PhD candidate in Macromolecular Chemistry and Physics at Fudan University. His research focuses on the design and application of nanomaterials for energy storage, including supercapacitors and rechargeable batteries.

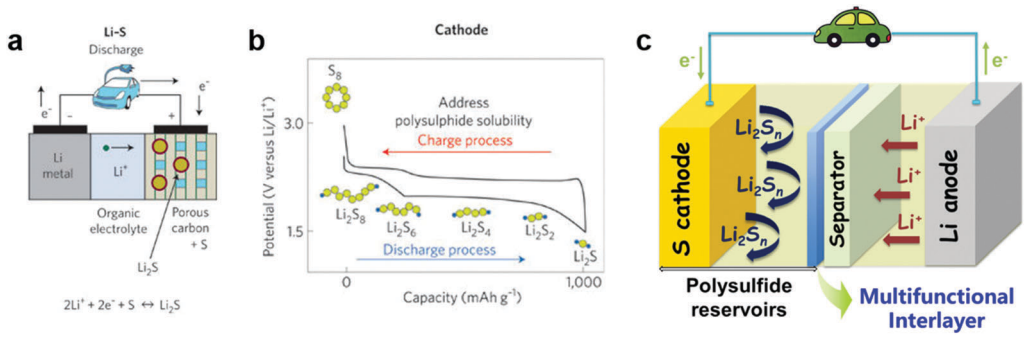

Fig. 1 General characteristics of the Li–S batteries: (a) schematic representations of a typical Li–S cell. (b) Illustration of polysulfide dissolution and the shuttling process in a Li–S battery during the recharge process. Reprinted with permission from ref. 11. Copyright 2011, Nature Publishing Group. (c) Schematic configuration of a Li–S battery with an interlayer inserted between the cathode and the separator.

devices, which are urgently needed in portable devices and electrical vehicles.[11–14] Li–S batteries usually comprise a sulfur cathode, lithium anode and separator saturated with organic electrolyte. As illustrated in Fig. 1a, the separator acts as a shield between the two electrodes that allows the transfer of lithium ions from the anode towards the cathode upon discharging, while the electrons move *via* the external circuit to the cathode. The overall reaction taking place between the anode and cathode can be summarized by the following reaction: $2Li + S \leftrightharpoons Li_2S$. During the discharge process, lithium ions generated from the oxidation reaction of the lithium anode migrate towards the cathode and react with solid-state sulfur. The reaction takes place by two steps: first forming liquid phase high-order polysulfides (Li_2S_8, Li_2S_6 and Li_2S_4) during the initial discharge process (2.4–2.2 V), followed by precipitation of low-order lithium disulfide and sulfide (Li_2S_2 or Li_2S, 2.2–1.8 V) in the cathode. In the charge process, a similar dissolution/precipitation procedure occurs.[1,15–17]

Although Li–S batteries have high theoretical capacity and great potential as good candidates for next-generation energy storage systems, there are significant problems that hinder their practical application, mainly the low utilization of sulfur and short cycling life.[18–23] The major challenges associated with Li–S batteries are listed as follows: (1) the insulating nature of sulfur. The poor electrical conductivity of elemental sulfur ($\sim 5 \times 10^{-30}$ S cm^{-1} at room temperature) hinders the electron transport in the cathode and leads to low utilization of active materials. (2) The polysulfide shuttle effect. The dissolution of intermediate polysulfide products formed during the charge/discharge processes and the shuttle behavior of polysulfides cause severe capacity fading and low Columbic efficiency (Fig. 1b). (3) Volume expansion of sulfur. A large volume change (80%) between sulfur and Li_2S during the charge/discharge processes results in the pulverization of the electrode materials and thus causes rapid capacity decay. (4) Formation of lithium dendrites. Corrosion reactions occur and lithium dendrites form on the surface of lithium metal upon cycling, resulting in poor cycling stability, low Columbic efficiency and a potential safety hazard.

To overcome the above issues, various efforts have been explored in the past few years to improve the conductivity of sulfur and hinder the dissolution of polysulfide into the electrolyte. A majority of studies involve combining sulfur with various types of host materials within the cathodes, including carbonaceous nanomaterials (*e.g.*, porous carbon, carbon nanotubes (CNTs), carbon nanofibers and graphene), polymers and metal compounds (*e.g.*, polypyrrole and TiO_2), as well as designing novel porous or yolk–shell architectures for the cathode.[24–37] These approaches enhance the electrical conductivity of the cathode and suppress the loss of soluble polysulfide intermediates during cycling, thereby enhancing the utilization of active materials and the cycling stability of Li–S batteries.

Along with this development, a practical concern has to be considered. The relatively low sulfur content and areal sulfur loading in these host cathode materials results in low energy density based on the whole cell, which cannot meet the requirement for practical applications. In addition, a complex

Tianxi Liu

Tianxi Liu received his PhD degree in Polymer Chemistry and Physics from the Changchun Institute of Applied Chemistry, Chinese Academy of Sciences in 1998. He was an Alexander von Humboldt Research Fellow from 1998 to 2000 at the University of Dortmund, Germany. He was a Research Associate from 2000 to 2001 and a Research Scientist from 2002 to 2004 at the Institute of Materials Research and Engineering (IMRE), Singapore. He joined as a full professor (since 2004) at the Department of Macromolecular Science, Fudan University, and then moved to the College of Materials Science and Engineering, Donghua University in 2016. He has published more than 230 articles in peer-reviewed journals (cited more than 7000 times with an H-index of 47). His current research interests include polymer nanocomposites, nanofibers and their composites, organic/inorganic hybrid materials, and new energy materials and devices.

synthesis process for designing the nanostructures of host materials and the poor reproducibility of such structures, which would become particularly acute for large-scale production, are huge impediments for achieving practical applications of these cathode materials in Li–S batteries.[2] Therefore, besides focusing on the modification 'inside' of the cathode, the design 'outside' of the cathode, such as cell configuration, could be a new strategy for improving the performance of the Li–S batteries. Significant progress has been achieved recently by designing novel cell configurations including polysulfide blocking interlayers, functional separators, anodic protection, and sandwiched or integrated cell structures, *etc.*[38–41] In particular, the introduction of a second barrier layer between the cathode and separator has been demonstrated to be an effective approach to inhibit polysulfide shuttling, resulting in enhanced cycling and rate performance of Li–S batteries (Fig. 1c). Herein, we present a comprehensive review of the recent developments of innovative configurations with a second barrier layer for Li–S batteries, with an emphasis on the interlayer insertion between the separator and sulfur cathode, separator modification and several state-of-the-art examples of interlayers in sandwiched/integrated configurations. It has to be mentioned that anodic protection such as employing hybrid anodes or introducing stable artificial interfaces to protect lithium metal anode is not included here, which can be found in other reviews.[42–44]

2 Cathodic interlayers

The insertion of a polysulfide-blocking interlayer between the separator and the sulfur cathode has been demonstrated to be a successful approach to significantly stabilize the lithium anode and fabricate high-performance Li–S batteries.[45–47] These interlayers with porous, conductive and flexible features could serve as barriers to improve the active material utilization, regulate the polysulfide shuttling, and maintain cycling stability and good efficiency, without involving complex synthesis or surface modification. First, the conductive interlayer decreases the internal charge transfer resistance and serves as an upper current collector, facilitating electron transfer in the cathode. Second, the nonpolar/polar interlayer localizes the soluble polysulfide species *via* physical or chemical interactions, efficiently blocking the migration of polysulfides from the S cathode towards the Li anode, thereby mitigating the passivation of Li anodes. Last but not least, the flexible structure of the interlayer is useful in reducing the volume change in the sulfur cathode, maintaining the structure integrity of electrode materials. Notably, porous carbon materials, carbon/metal compounds and conductive polymers have been employed for interlayers between the separator and the S cathode, and thereby greatly enhanced performance of Li–S batteries is achieved (Table 1).

2.1 Carbon-based interlayers

Carbon materials are the most popular materials for the interlayers used in Li–S batteries. It is believed that a thin interlayer of carbon materials can not only localize the soluble polysulfides and prevent the shuttle effect but also works as an upper current collector to improve the utilization of the active material. In 2012, Manthiram *et al.* innovatively proposed a new cell configuration using microporous carbon paper as an interlayer covered on the surface of a bare sulfur cathode (Fig. 2a and b).[45] The microporous carbon paper can effectively decrease the resistance of sulfur cathodes, and the carbon interlayer with micropores facilitates the adsorption of soluble polysulfides in the electrolyte and makes them available to be reutilized even during long cycles. In addition, this bifunctional carbon interlayer can be treated as a second current collector for accommodating the migrating active material from sulfur cathodes. The cell with a microporous carbon interlayer delivered an excellent capacity above 1000 mA h g^{-1} at 100 cycles at a current density of 1675 mA g^{-1} within a voltage window of 1.5 and 2.8 V (*vs.* Li^+/Li) and a high average Columbic efficiency of 97.6% (Fig. 2c). Subsequently, a number of carbon-based interlayers have been investigated and found to improve the cycling stability of Li–S cells, including CNT paper,[48–51] treated carbon paper,[52] graphene films,[53–56] a carbonized eggshell membrane,[57] carbonized Kimwipes paper,[58,59] electrospun carbon nanofibers,[60–64] carbonized cellulose paper,[65,66] mesoporous carbon,[67,68] carbon fiber cloth,[69] and carbon aerogels.[70] A reduced graphene oxide based film was sandwiched between a sulfur cathode and the separator, acting as a shuttle inhibitor for the polysulfides. The Li–S cell with such a configuration showed an initial discharge capacity of 1260 mA h g^{-1} at a current density of 200 mA g^{-1} and the capacity remains at 895 mA h g^{-1} after 100 cycles.[53] Kim *et al.* demonstrated that graphene oxide paper combined with conductive CNTs could improve the blocking effect and result in better cell performance.[55] In another case, a carbon fiber cloth interlayer with a high electric conductivity, a large surface area and excellent flexibility was directly inserted between a sulfur cathode and a separator to trap the soluble lithium polysulfide intermediates.[69] A cell with this interlayer delivered a high reversible capacity (>560 mA h g^{-1}) at a large current density of 33.45 mA cm^{-2} over 1000 cycles between 2.8 and 1.6 V (*vs.* Li^+/Li). Moreover, a mechanically robust, electrically conductive carbon hybrid aerogel with aligned and interconnected pores was prepared and investigated as an interlayer for Li–S batteries.[70] The hierarchical cross-linked networks constructed by graphene sheets and CNTs can act as an ''internet'' to capture the polysulfide, while the micro- and nano-pores inside the aerogel can facilitate quick penetration of the electrolyte and rapid transport of lithium ions. Due to the advantages of the unique structure and excellent accommodation of the volume change in the active materials, a high specific capacity of 1309 mA h g^{-1} at 0.2C was achieved for the assembled Li–S batteries, coupled with good rate performance and long-term cycling stability (78% capacity retention after 600 cycles at 4C). However, due to the weak physical adsorbing ability of nonpolar carbon for highly polar polysulfides, the long-term cycling performance of these pure carbon interlayers for Li–S batteries still needs to be improved. Therefore, strong chemical binding of lithium polysulfides to the carbon matrix is fundamentally essential for further mitigation of polysulfide shuttling.

Table 1 Comparison of Li–S cell performance with various interlayers

Interlayers	Electrolyte[a]	Initial discharge capacity[b] (mA h g^{-1})	Voltage window (V)	Cycling performance: final discharge capacity (mA h g^{-1}) (capacity retention)/ cycle number/current density	Ref.
Microporous carbon paper	1.85 M $LiCF_3SO_3$ + 0.1 M $LiNO_3$ in DOL/DME (1 : 1, v : v)	1367/1C	1.5–2.8	1000 (85%)/100/1C 846/150/2C	45
Multiwalled carbon nanotube paper	1.85 M $LiCF_3SO_3$ + 0.1 M $LiNO_3$ in DOL/DME (1 : 1, v : v)	1446/0.2C	1.5–2.8	962/50/0.2C 804/100/1C	48
Carbon nanotube-loaded glass-filter composite paper	1 M LiTFSI + 0.2 M $LiNO_3$ in DOL/DME (1 : 1, v : v)	1112/0.2C	1.5–2.8	803 (73%)/230/0.2C 743 (87%)/300/1C	49
Treated carbon paper	1 M $LiCF_3SO_3$ + 0.1 M $LiNO_3$ in DOL/DME (1 : 1, v : v)	1651/0.2C	1.5–2.8	900 (54%)/50/0.2C 780 (64%)/50/1C	52
Reduced graphene oxide film	1 M LiTFSI in DOL/DME (1 : 1, v : v)	1260/0.1C	1.0–3.0	895/100/0.1C	53
Porous graphene oxide/carbon nanotube hybrid films	1 M LiTFSI + 1 wt% $LiNO_3$ in DOL/DME (1 : 1, v : v)	1600/0.2C	1.5–2.8	670/100/0.2C 441/300/1C	55
Graphene oxide membrane	1 M LiTFSI + 0.1 M $LiNO_3$ in DOL/DME (1 : 1, v : v)	1182/0.5C	1.8–2.8	835/100/0.5C 750 (70%)/400/1C	56
Carbonized egg shell membrane	1.5 M sulfur in DOL/DME (1 : 1, v : v)	1327/0.1C	1.8–3.0	1000/100/0.1C	57
Carbonized Kimwipes paper	1.85 M $LiCF_3SO_3$ + 0.1 M $LiNO_3$ in DOL/DME (1 : 1, v : v)	1235/0.2C	1.8–2.8	1044 (85%)/100/0.2C 824 (71%)/100/2C	58
Electrospun polyacrylonitrile-based carbon nanofiber	1.85 M $LiCF_3SO_3$ + 0.1 M $LiNO_3$ in DOL/DME (1 : 1, v : v)	1549/0.2C	1.8–2.8	1146 (74%)/100/0.2C 948 (90%)/100/1C	60
Electrospun polyimide-based carbon nanofiber	1 M LiTFSI + 0.1 wt% $LiNO_3$ in DOL/DME (1 : 1, v : v)	1224/0.1C	1.5–3.0	906 (73%)/100/0.1C	61
Carbon fiber cloth	1 M LiTFSI + 0.4 M $LiNO_3$ in DOL/DME (1 : 1, v : v)	1087/1C	1.6–2.8	1033 (95%)/100/1C 560/1000/5C	69
Carbon nanotube/graphene hybrid aerogel	1 M LiTFSI + 0.1 M $LiNO_3$ in DOL/DME (1 : 1, v : v)	1309/0.2C	1.7–3.0	1021 (78%)/100/1C 597/600/4C	70
N,O-Doped porous carbon film	1 M LiTFSI + 0.1 M $LiNO_3$ in DOL/DME (1 : 1, v : v)	1250/0.5C	1.8–3.0	700/300/1C 650/300/5C	77
Sulfur-doped microporous carbon	1 M LiTFSI + 0.1 M $LiNO_3$ in DOL/DME (1 : 1, v : v)	1544/0.2C	1.7–2.8	977 (63%)/200/0.2C 720/500/2C	79
Sulfur/nitrogen dual-doped graphene	1 M LiTFSI + 1 wt% $LiNO_3$ in DOL/DME (1 : 1, v : v)	1030/0.5C	1.5–3.0	612 (79%)/250/2C 326/1000/8C	80
Fe_3C/carbon nanofiber webs	1 M LiTFSI + 1 wt% $LiNO_3$ in DOL/DME (1 : 1, v : v)	1177/0.2C	1.5–2.8	893 (76%)/100/0.2C	87
Graphene/TiO_2 film	1 M LiTFSI + 1 wt% $LiNO_3$ in DOL/DME (1 : 1, v : v)	1050/0.5C	1.8–2.8	1040/300/0.5C 535/1000/3C	88
TiO_2/carbon nanotube paper	1 M LiTFSI + 0.1 M $LiNO_3$ in DOL/DME (1 : 1, v : v)	1085/0.5C	1.7–3.0	576/250/0.5C	89
TiO_2 decorated carbon nanofibers	1 M LiTFSI + 1 wt% $LiNO_3$ in DOL/DME (1 : 1, v : v)	935/1C	1.7–2.8	692 (74%)/500/1C	90
TiO_2/N-doped porous carbon	1 M LiTFSI + 0.5 M $LiNO_3$ in DOL/DME (1 : 1, v : v)	875/0.1C	1.7–2.8	805 (92%)/100/0.1C 670/300/1C	91
V_2O_5 decorated carbon nanofiber	1 M LiTFSI + 1 wt% $LiNO_3$ in DOL/DME (1 : 1, v : v)	1059/0.3C	1.7–2.8	76%/250/0.3C 71%/1000/3C	93
Ultrathin MnO_2/graphene oxide/carbon nanotube	1 M LiTFSI + 0.2 M $LiNO_3$ in DOL/DME (1 : 1, v : v)	1055/0.5C	1.8–2.6	80%/200/0.5C 293/2500/1C	94
1D graphene nanoscrolls/MnO_2 nanowires	1 M LiTFSI + 0.1 M $LiNO_3$ in DOL/DME (1 : 1, v : v)	1544/0.1C	1.5–2.8	545/400/4C	95
Porous CoS_2/carbon paper	1 M LiTFSI + 0.1 M $LiNO_3$ in DOL/DME (1 : 1, v : v)	1239/0.2C	1.7–2.8	818/200/0.2C	97
WS_2/carbon cloth	1 M LiTFSI + 0.1 M $LiNO_3$ in DOL/DME (1 : 1, v : v)	1454/0.02C	1.7–2.8	72%/500/0.5C	98
TiO_2–TiN heterostructure/graphene	1 M LiTFSI + 2 wt% $LiNO_3$ in DOL/DME (1 : 1, v : v)	1008/0.3C	1.7–2.8	927 (92%)/300/0.3C 73%/2000/1C	102
Functionalized boron nitride nanosheet/graphene composite	1 M LiTFSI + 5 wt% $LiNO_3$ in DOL/DME (1 : 1, v : v)	1125/0.2C	1.6–2.8	700/1000/1C 558/1000/3C	107
Polypyrrole nanoparticles	1 M LiTFSI in DOL/DME/PYR14TFSI (2 : 2 : 1, v : v : v)	719/0.2C	1.5–2.8	846/200/0.2C 533/300/2C	110
Polypyrrole nanotube film	1 M LiTFSI in DOL/DME (1 : 1, v : v)	1102/0.5C	1.8–2.8	712/300/0.5C	111

[a] LiTFSI: bis-trifluoromethane sulfonylimide; DOL: 1,3-dioxolane; DME: 1,2-dimethoxyethane. [b] 1C = 1675 mA g^{-1}.

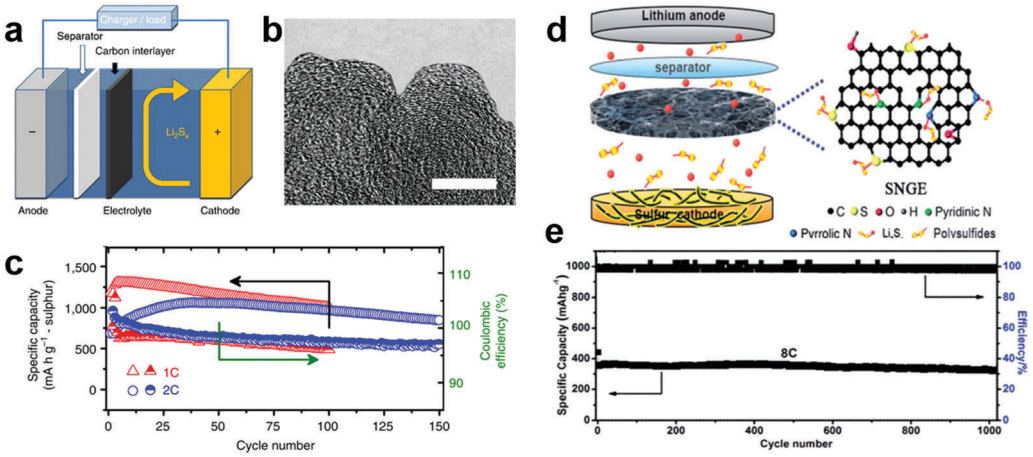

Fig. 2 Li–S batteries with carbon-based interlayers. (a) Schematic configuration of the Li–S battery with a microporous carbon interlayer inserted between the electrode and the separator, (b) transmission electron microscope image of the microporous carbon, (c) cycle life and Coulombic efficiency of the cell with microporous carbon paper at 1C and 2C for 150 cycles. Reprinted with permission from ref. 45. Copyright 2012, Nature Publishing Group. (d) Schematic representation of the assembled Li–S batteries with a sulfur–nitrogen dual-doped graphene (SNGE) interlayer, and the corresponding prolonged cycling performance at a rate of 8C over 1000 cycles. Reprinted with permission from ref. 80. Copyright 2016, Royal Society of Chemistry.

Recent studies have shown that the surface chemical modification of carbon materials by heteroatom doping (such as O, N, B and S) can improve the immobilization of lithium polysulfides through strong chemical binding.[71–76] It has been reported that N-doped graphene with clustered pyridinic N-dopants could effectively attract and tightly anchor soluble polysulfides by means of their large binding energies, which is due to the enhanced attraction between Li ions in polysulfides and pyridinic N-dopants, as well as the additional attraction between the sulfuric anions in polysulfides and Li ions captured by pyridinic N-dopants.[72] Thus, heteroatom doped carbon materials were applied as interlayers for Li–S batteries. N,O-doped porous carbon film (GFC film) was reported as a superior conductive interlayer for improving the performance of Li–S batteries.[77] By inserting the N,O-doped GFC film, the battery delivered a capacity of $\sim$700 mA h g^{-1} after 300 cycles at 1C. Even at 5C, it exhibited a reversible capacity of more than 650 mA h g^{-1}. Sulfur atoms are also one of the most promising heteroatoms that can enhance the conductivity of carbon, increase the affinity between polysulfides and carbon frameworks, and facilitate immobilization of polysulfide ions to improve the electrochemical performance of Li–S batteries.[78] Sulfur-doped microporous carbon (SMPC) using a luffa sponge as the precursor was developed as an interlayer between a conventional sulfur cathode and separator.[79] The SMPC showed a unique microporous carbon framework, large specific surface area (3211.2 mg^2 g^{-1}), high pore volume (1.72 cm^3 g^{-1}), good electrical conductivity (1.89 S cm^{-1}) and *in situ* S-doping (2.72 at%). The Li–S cells containing this SMPC interlayer exhibited a large reversible capacity of 1544.2 mA h g^{-1} at 0.2C, an excellent rate capacity of 781.2 mA h g^{-1} at 5C, and superior long-term cycling stability over 500 cycles at 2C. A new design using a porous-CNT/S cathode coupled with a lightweight porous sulfur/nitrogen dual-doped graphene (SNGE) interlayer in a Li–S cell was investigated.[80] The high heteroatom doping concentration endows the SNGE with abundant chemical adsorption sites, which is favorable for trapping the migrating lithium polysulfides and suppressing the shuttling of lithium polysulfides (Fig. 2d). The cell with this special interlayer can deliver a reversible specific capacity of $\sim$1460 mA h g^{-1} at 0.25C and ultrahigh cycling stability when cycled at 8C for 1000 cycles, exhibiting a capacity degradation rate of 0.01% per cycle (Fig. 2e). Similarly, another report showed that N and S co-doping could significantly enhance the binding of lithium polysulfides as compared to the undoped or single N/S-doped graphene, thus leading to better cycle performance.[81] Therefore, doping with miscellaneous elements is an effective method to enhance the interaction between the polysulfides and carbon matrix, thus improving the cycling life of Li–S batteries.

2.2 Carbon/metal compound-based interlayers

Although porous carbon materials could adsorb lithium polysulfides physically, the long-term stability of the Li–S batteries still needs improvement since the polysulfides would unavoidably be desorbed from these porous carbon materials due to the relatively weak interaction between them. To further modulate the binding energy with polysulfides and increase the tap density of electrodes, nanostructured polar inorganic compounds, such as transition-metal oxides, sulfides, and carbides have emerged as polar host materials toward lithium polysulfides.[31,82,83] These compounds (such as TiO_2, TiC, Ti_4O_7, MnO_2, and CoS_2) have much stronger adsorption ability to polysulfides and render the Li–S cells with high sulfur utilization and long life span.[84–86] However, utilization of metal oxides for the interlayer still remains a challenge since the introduced oxides with intrinsic poor conductivity would bring extra electronic and ionic resistances, thus making it difficult to reactivate the trapped polysulfides within the interlayer and reversely deteriorating the Li–S battery performance. Hence, it seems to be more efficient and practical to make hybrid interlayers by compounding metal oxides with highly conductive carbon. Compared with pure carbon-based

interlayers, carbon interlayers modified with metal compounds (*e.g.*, Fe_3C,[87] TiO_2,[88–92] V_2O_5,[93] MnO_2,[94–96] CoS_2,[97] WS_2[98]) can more effectively confine the dissolved polysulfides. The carbon matrix adsorbs the polysulfides physically due to the porosity of carbon materials, while the supported metal compounds can further capture the polysulfides by chemical combination.

TiO_2 has been demonstrated to be a promising compound to improve the cycling stability of Li–S batteries, and it is believed to be an electrostatic attraction (S–Ti–O) that improves the surface adsorption of polysulfides on the TiO_2.[99,100] A graphene/TiO_2 film was developed as an interlayer for Li–S batteries, which accounted for only ~7.8 wt% of the whole cathode (Fig. 3a and b).[88] It was found that the application of the graphene/TiO_2 film as an interlayer enabled the sulfur cathode to deliver a reversible specific capacity of ~1040 mA h g^{-1} over 300 cycles at 0.5C. When they were cycled at higher rates, these cathodes exhibited ultrahigh cycling abilities, with a capacity degradation rate of 0.01% and 0.018% per cycle over 1000 cycles at 2 and 3C, respectively (Fig. 3c). Subsequently, TiO_2 nanoparticles hybridized with CNT paper,[89] carbon nanofibers,[90] and N-doping porous carbon[91] have also been applied as interlayers for Li–S batteries and exhibited improved cycling stability. The effects of the multifunctional TiO_2/carbon-based interlayer for Li–S batteries are elucidated by the following aspects. First, the TiO_2/carbon barrier physically blocks the diffusion of lithium polysulfides to the lithium anode. This could restrict the *in situ* transformation of active materials to lithium polysulfides on the cathode surface, and also block existing lithium polysulfides from reacting with the lithium anode. Second, the positively charged TiO_2 on the carbon materials attracts the negatively charged polysulfide anions by electrostatic adsorption. The interaction between Lewis-acidic Ti(IV) centers and the basic polysulfides attracts the escaped lithium polysulfides. Most importantly, TiO_2 chemically adsorbs sulfur species by forming Ti–S and S–O bonds. The DFT calculation results show that strong Ti–S interactions exist in all lithium polysulfide structures, which could result from the similar ionic bonding properties of TiO_2 and Li_2S_n.[85,101] More recently, Yang *et al.* designed a twinborn TiO_2–TiN heterostructure loaded onto graphene with the resulting hybrid being a thin but highly effective polysulfide blocking interlayer.[102] This heterostructure combines the merits of highly adsorptive TiO_2 with conducting TiN, where lithium polysulfides are strongly trapped by TiO_2 and then smoothly diffused across the smooth TiO_2/TiN interface to TiN that promotes lithium polysulfides nucleation and fast conversion into insoluble Li_2S. The assembled battery showed a high specific capacity, high rate capability and ultra-long cycling performance. A low current density (0.3C) test showed a capacity of 927 mA h g^{-1} after 300 cycles (92% capacity retention). More promisingly, in ultra-long cycling tests (up to 2000 cycles at 1C), capacity retentions of 73% and 67% were respectively achieved for sulfur loadings of 3.1 and 4.3 mg cm^{-2}. The unique heterostructure design and the simple preparation technology are expected to promote the practical use of Li–S batteries with outstanding capacity and cycling performances.

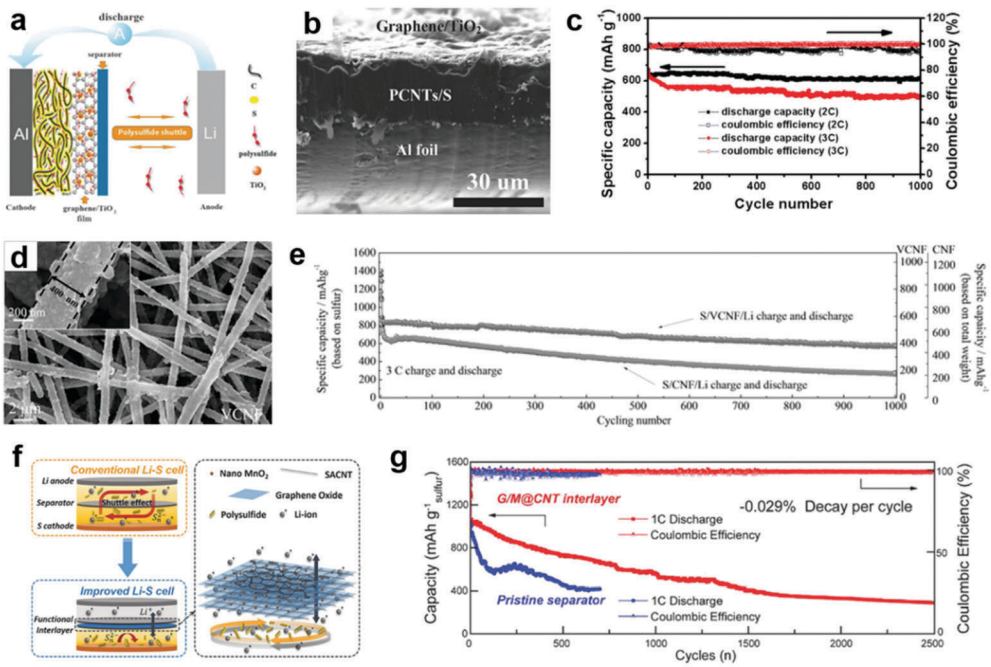

Fig. 3 Li–S batteries with carbon/metal compound-based interlayers. (a) Schematic configuration for a Li–S battery with a graphene/TiO_2 interlayer, (b) typical cross-sectional scanning electron microscopy (SEM) images of a fresh cathode with a graphene/TiO_2 interlayer, and (c) cycling stability of a cathode with a graphene/TiO_2 interlayer at 2 and 3C. Reprinted with permission from ref. 88. Copyright 2015, Wiley-VCH. (d) Typical SEM image of a V_2O_5-decorated carbon nanofiber (VCNF), and (e) long term cycling performance of S/CNF/Li and S/VCNF/Li cells at 3C. Reprinted with permission from ref. 93. Copyright 2017, Wiley-VCH. (f) Schematic diagram of an electrode structure with a functional MnO_2/graphene oxide/carbon nanotube (G/M@CNT) interlayer, and (g) prolonged cycling performances of electrodes with/without the G/M@CNT interlayer at 1C. Reprinted with permission from ref. 94. Copyright 2017, Wiley-VCH.

The mechanism of V_2O_5 and MnO_2 for polysulfide trapping is quite different from TiO_2, which is decided by the different redox potentials of these oxides. The higher redox potentials (>3 V) of V_2O_5 and MnO_2 could oxidize polysulfides and anchor the products, while the lower redox potential (<2 V) of TiO_2 presents only physical adsorption ability (S–Ti–O).[83] Recently, Cui and co-workers calculated that layered structure V_2O_5 had strong chemical interaction with Li_2S_n clusters.[103] Nazar *et al.* proposed that V_2O_5 could act as a redox mediator to oxidize polysulfides to thiosulfate/polythionate groups and chemically bond them on the surface of reduced metal oxide.[83] As expected, V_2O_5 delivers a high redox potential of 4.0–2.0 V (*vs.* Li/Li^+) and a theoretical capacity of 296 mA h g^{-1}, which is competitive to be the most suitable decoration material matching with a pure carbon interlayer.[104] Based on the above mentioned theory, a novel V_2O_5 decorated carbon nanofiber (VCNF) membrane was synthesized and utilized as an interlayer in Li–S batteries (Fig. 3d).[93] The well-decorated V_2O_5 component not only anchors polysulfides through strong chemical interactions, but also effectively suppresses the cell's self-discharge behavior due to its voltage regulation function. As a result, the Li–S battery with a VCNF interlayer exhibited a high rate capability (1432, 1059, 953, 849, 757 and 709 mA h g^{-1} at 0.1, 0.3, 0.5, 1, 3 and 5C, respectively) and excellent capacity retentions at both low and high current densities with 76% after 250 cycles at 0.3C and 71% after 1000 cycles at 3C, respectively (Fig. 3e). It has been recently reported that the oxygen groups from MnO_2 can react with polysulfides to form surface-bound intermediates, *i.e.*, $S_2O_3^{2-}$ species, preventing polysulfide dissolution, and prompt the surface adsorption of polysulfides because it possesses a strong electrostatic attraction (S–Mn–O) to sulfur species.[82] Ultrathin MnO_2/graphene oxide/carbon nanotube (G/M@CNT) interlayers were developed as efficient polysulfide-trapping shields for high-performance Li–S batteries (Fig. 3f).[94] The G/M@CNT interlayer provides a physical shield against polysulfide shuttling and chemical adsorption of polysulfides by MnO_2 nanoparticles and graphene oxide sheets. The synergetic effect of the G/M@CNT interlayer enables the production of Li–S cells with high sulfur loadings (60–80 wt%), a low capacity decay rate ($\sim$0.029% per cycle over 2500 cycles at 1C), high rate performance (747 mA h g^{-1} at a charge rate of 10C), and a low self-discharge rate with high capacity retention (Fig. 3g). A free-standing hybrid interlayer composed of interlaced 1D graphene nanoscrolls and MnO_2 nanowires was fabricated for Li–S batteries.[95] The well-designed hybrid interlayer not only exhibited enhanced electronic and ionic conductivities, but also manifested strong physical/chemical interactions to control the shuttling of polysulfides and ensure their continuous reutilization. As a result, the assembled cell retained a reversible discharge capacity of 545 mA h g^{-1} even after 400 cycles at the high 4C rate, corresponding to an ultralow capacity decay of 0.08% per cycle.

With the demand for strong interaction with polysulfides and high conductivity, metal sulfides have been applied in interlayers for Li–S batteries. Metal sulfides have several intrinsic benefits: (1) the strong sulfiphilic property to sulfur-containing species and (2) low lithiation voltages *vs.* Li/Li^+, which can avoid overlap in the working voltage window of Li–S batteries.[31] Pyrite-type CoS_2 has been proven to have high catalytic activity in polysulfide reduction and possesses an appreciable conductivity of 6.7×10^3 S cm^{-1} at 300 K. The formed Li–S bond between CoS_2 and chain Li_2S_n/Li_2S can effectively alleviate the diffusion of polysulfides into the electrolyte. In particular, the weak van der Waals force between CoS_2 and Li_2S_n/Li_2S can well preserve the integrity of the Li–S bond in Li_2S_n/Li_2S.[105] Inspired by this, hierarchically porous CoS_2/carbon paper was applied as an interlayer for capturing polysulfides through physical adsorption and chemical bonding in a working Li–S cell.[97] The sulfur cathode delivered a high initial capacity of 1239.5 mA h g^{-1} at 0.2C and retained a reversible capacity of 818 mA h g^{-1} after 200 cycles. More recently, Goodenough *et al.* reported a Li–S cell with excellent cycle life and rate performance by using interlayers of tungsten disulfide (WS_2) supported on carbon cloth.[98] WS_2 is a well-known catalyst used for hydrodesulfurization because of its strong adsorption of sulfur and sulfides, thus providing superior adsorption of soluble polysulfides.[106] The polysulfides trapped by the dangling sulfur bonds on the edges of the WS_2 particles disproportionate into lower-order polysulfides before being reduced to Li_2S by electrons from the anode *via* the carbon cloth. The carbon cloth acts as a physical barrier blocking polysulfide migration and provides fast electron transfer between the cathode current collector, while the supported WS_2 particles adsorb soluble polysulfides. As a result, the WS_2/S electrode showed an excellent cycling stability with 72.5% capacity retention at the 500th cycle (0.5C) and rate capability (701.8 mA h g^{-1} at a 5.0C rate). Functionalized boron nitride nanosheets (FBNs) with positively charged amino groups have also been proved to be promising interlayer materials, since the polysulfides can be trapped by these positively charged surfaces and easily released during discharging and charging processes.[107] A thin film of a FBN/graphene composite as an interlayer can effectively decrease the charge transfer resistance, entrap the polysulfides on the cathode surface, and exhibit ultrahigh cycling abilities as compared to the batteries without any interlayer. The interlayers suppress the polysulfide shuttle leading to a low capacity degradation rate of 0.0067% and 0.0037% per cycle, measured over 1000 cycles at current densities of 1 and 3C, respectively.

2.3 Polymer-based interlayers

Conductive polymer interlayers have also been developed to mitigate the shuttle effect and to protect the Li anode to improve the cycling stability of Li–S batteries. It is reported that the proton-doped conductive polymers can adsorb polysulfide more effectively during the charge/discharge process, *via* H-bonds between the polymer and polysulfide anions.[108] Meanwhile, the conductive polymers are both electronically and ionically conductive, which is beneficial for reducing the resistance and enhancing the rate capability of the Li–S cell. Furthermore, the conductive polymers themselves are electrochemically active, which can provide some capacity for the cell.[109] Thus conductive polymers are suitable to be used as a functional interlayer for Li–S batteries. Polypyrrole-based interlayers between the Li anode and the S cathode were fabricated to enhance the cycling

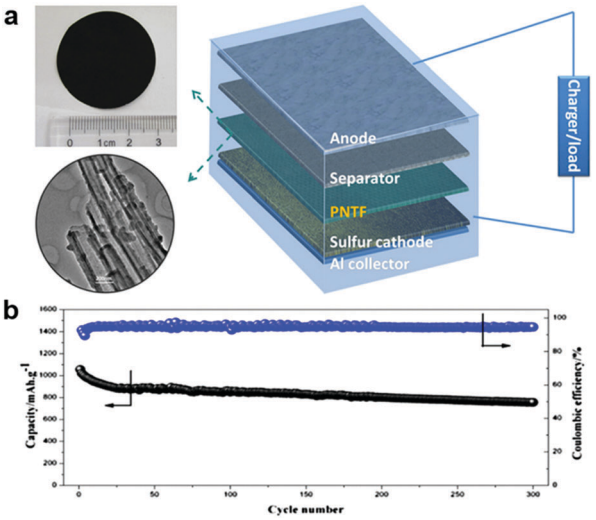

Fig. 4 Li–S batteries with polymer-based interlayers. (a) Schematic cell configuration of rechargeable Li–S batteries with a polypyrrole nanotube film (PNTF) interlayer, and the corresponding photograph and TEM image of PNTF, (b) the prolonged cycle performance of Li–S batteries with PNTF at 0.5C. Reprinted with permission from ref. 111. Copyright 2015, Elsevier.

performance of the Li–S batteries (Fig. 4a).[110,111] Because of the adsorption effect between polypyrrole and lithium polysulfides and the conductivity of polypyrrole films, the polypyrrole functional interlayer could inhibit the dissolution and migration of lithium polysulfides in the electrolyte, and buffer the volume expansion of the sulfur cathode during the charge/discharge process. The Li–S cell containing the polypyrrole nanotube interlayer exhibited a high specific capacity (>1100 mA h g^{-1}), good cycling stability (>700 mA h g^{-1} over 300 cycles) and high Columbic efficiency (about 92%) in the range of 2.8–1.8 V (*vs.* Li/Li^+) (Fig. 4b).[111] Polyvinylidene fluoride (PVDF) membranes have also received attention in battery applications due to their good chemical stability, low thickness, appropriate porosity and good mechanical strength. PVDF is chosen to form the interlayer backbone, which is good for Li^+ dissociation and transport due to the good electrolyte miscibility and high dielectric coefficient of $–CH_2–CF_2–$chains.[112] A nano-Li^+-channel interlayer was successfully prepared by swelling the PVDF dense membrane with an electrolyte to form an inter-connected ion transport network among the molecular chains.[113] Its special ion transport channels could selectively separate the Li^+ and polysulfide and exhibited better Li^+/polysulfide selective permeability when compared with the microporous polyethylene membrane. Consequently, the nano-Li^+-channel interlayer can confine the lithium polysulfide shuttling, leading to a high specific capacity between 1.5 and 2.8 V. However, the PVDF membrane has a negative effect on the electronic conduction, which results in low specific capacity and poor cycling stability of the Li–S batteries. Hence, a carbon nanofiber modified PVDF (CNF/PVDF) composite membrane was designed and used as an interlayer for Li–S batteries.[114] The PVDF membrane could effectively separate dissolved lithium polysulfide, while the high electronic conductive CNF not only reduced the internal resistance in the sulfur cathode but also helped immobilize the polysulfide through its abundant nano-spaces. The resulting Li–S battery assembled with the CNF/PVDF composite membrane effectively solves the polysulfide permeation problem and exhibits excellent electrochemical performance. It was further found that the CNF/PVDF electrode had an excellent cycling stability and retained a capacity of 768.6 mA h g^{-1} with a Columbic efficiency above 99% over 200 cycles at 0.5C, which was more than twice that of a cell without CNF/PVDF (374 mA h g^{-1}). A novel multi-functional interlayer composed of an outer cyclized-polyacrylonitrile (PAN) network and inner carbon nanofiber skeleton (CP@CNF) was developed based on dip-coating an electrospun CNF film in PAN solution and subsequent thermal cyclization treatment.[115] The CNF skeleton with superior conductivity serves as a platform for sulfur reutilization while the conductive cyclized-PAN network possessing abundant pyridinic nitrogen groups acts as the polar host to capture polysulfides and confine their dissolution and shuttling. The assembled Li–S batteries with CP@CNF interlayers exhibited enhanced rate performance and cycling stability with a high capacity retention of 74% at 0.3C after 200 cycles.

Considering the specific electrochemical process of Li–S batteries, the concept of introducing an interlayer brings a new configuration for high-performance Li–S batteries. Generally, interlayers should have porous, conductive, and flexible features, which can function as a polysulfide inhibitor, current collector and structural stabilizer for the battery system. First, the porous interlayers can adsorb the polysulfides generated during the charge/discharge process, mitigating the shuttle effect and alleviating the corrosion of the lithium anode. To improve the efficiency as a polysulfide inhibitor, rational designs of porous structures and the surface properties of the interlayer are highly required. One ideal porous structure for the interlayer is a hierarchical porous structure with a micro–meso–macroporous interconnected structure, which is favorable for both electrolyte permeation and polysulfide adsorption. Besides, gradient or layered structures are also promising to slow down the polysulfide permeation process through the interlayer. Furthermore, due to the strong affinity with polysulfides, hetero-atom doping and polar inorganic compounds, such as transitional-metal oxides, sulfides, and carbides are promising candidates for interlayers with high trapping efficiency for polysulfides. Second, in order to reduce the charge transfer resistance for the sulfur cathode, an interlayer with higher conductivity and better contact with the cathode are strongly considered. The interlayer acted as an upper current collector to facilitate the sulfur utilization, contributing to a higher capacity with better cycling stability. For pursuing high conductivity and intimate contact with the sulfur cathode, a hybrid structure with a metal framework and carbon nanomaterials decorated on the surface of the metal framework is greatly recommended, in which the metal framework provides a long-range conducting network while the carbon nanomaterials ensure the intimate contact with the cathode. Last, the flexibility of the interlayer also ensured the robust mechanical property, which accommodated the volume change in the sulfur materials and preserved the structural stability of the sulfur cathode.

Hence, a highly stable, self-woven, and self-standing skeleton, such as flexible membranes constructed by long CNTs and carbon nanofibers, is suitable for the design of an interlayer with enhanced structural stability. In summary, the wise combination of good mechanical stability with a highly conductive framework, and a rational design of a porous structure together with suitable surface modification is necessary for the next-generation of high-performance interlayers for Li–S batteries.

3 Functionalized separators

The separator is one essential part in an electrochemical cell, playing an important role in preventing internal short-circuit and maintaining the ion diffusion pathways.[116] During the cycling processes in Li–S batteries, the dissolved polysulfides in the electrolyte would inevitably diffuse through the separator and cause parasitic reactions with the anode (lithium metal), thus resulting in serious degradation of the anode and rapid capacity decline of the batteries. As a result, an ideal separator for Li–S batteries is expected to not only have a good ionic conductivity after adsorbing the liquid electrolyte, but also suppress the migration of polysulfides during cycling. Suitable modification of separators has been proved to be an effective method to suppress the shuttling behavior of polysulfides and to enhance the performance of Li–S batteries.[117–120] In this section, we summarize recent progress in the development of novel separators for Li–S batteries. The strategies used for the prevention of polysulfide shuttling through the separator can be roughly categorized into two classes: (1) functionalization of polyolefin separators with coatings capable of suppressing polysulfide diffusion, and (2) use of other separators, such as functional polymeric and ceramic membranes, that provide barrier properties against polysulfides.

3.1 Functionalized polyolefin-based separators

Functionalization of traditional polyolefin-based separators with an additional barrier layer is a simple and straightforward approach to alleviate the shuttle effect in Li–S batteries. The ionic conductivity and selectivity are two important factors for an ideal modified separator, where fast transfer of lithium ions is achieved and polysulfide shuttling is restrained. For this purpose, a variety of materials (including carbon,[121–134] metal oxides,[135–146] polymer,[147–151] and their composites *etc.*) have been developed and utilized for separator modification, and the promising functionalized separators are discussed with an emphasis on the strategies and resultant performance of Li–S batteries.

3.1.1 Carbon modified polyolefin separators. Carbon materials are commonly used for separator modification owing to their unique advantages including cost-effectiveness, large specific surface area, excellent electrical conductivity and thermal stability, *etc.* The conductive, porous structure of carbon materials can effectively adsorb the dissolved polysulfides and alleviate the shuttle effect. For instance, by integrating the commercial conductive carbon black (Super P carbon) and a polymeric separator (Celgard separator), a light-weight carbon-coated separator was facilely prepared and proved to be an effective polysulfide-diffusion barrier.[121] On one hand, this conductive carbon-coating can serve as an ''upper'' current collector to offer additional electron pathways for the intercepted sulfur materials. On the other hand, the carbon-coating layer can suppress the free diffusion of polysulfides for high sulfur utilization. As a consequence, the cells with a carbon-coated separator and pure sulfur cathode delivered a high initial discharge capacity of 1400 mA h g^{-1} with reversible capacity of 828 mA h g^{-1} after 200 cycles at a C/5 rate, and a high Columbic efficiency of about 98% in an electrolyte of 1.85 M $LiCF_3SO_3$ and 0.1 M $LiNO_3$ in DOL/DME (1 : 1, v : v). Moreover, the resulting carbon-coated separator is only 0.2 mg cm^{-2} while the weight of the Celgard separator is 1.0 mg cm^{-2}, which avoids the unnecessary increase of cell weight and unsatisfactory decrease of energy density. Following a similar strategy, a straightforward coating modification of the commercial separator with mesoporous carbon is also proved effective to enhance the cycling performance of Li–S batteries.[124] The mesoporous structure of carbon can not only provide numerous void-spaces for the physical trapping and confinement of polysulfides, but also accommodate volume variation of the sulfur cathode during the cycling process. The resulting Li–S cell with a mesoporous carbon-coated separator exhibited a high reversible capacity of 723 mA h g^{-1} after 500 cycles at 0.5C, with a degradation rate of only 0.081% per cycle with an electrolyte of 1 M LiTFSI and 0.25 M $LiNO_3$ in DOL/DME (1 : 1, v : v). Apart from carbon black and mesoporous carbon, carbon nanomaterials such as CNTs and graphene are also employed for separator modification. For example, a single-wall carbon nanotube (SWCNT)-modulated separator that can be prepared in various sizes using an vacuum-filtration approach, showed great potential as a functional separator for effective stabilization of a high-loading sulfur cathode in Li–S batteries (Fig. 5a).[129] The long-range SWCNTs connect with each other and form a crisscrossing spider net-like network coating on one side of a Celgard separator that greatly mitigates the diffusion of polysulfides (Fig. 5b). Besides, from the micropore analyses, SWCNTs possess a high micropore surface area of 189 $m^2 g^{-1}$ with small micropore sizes mainly in the range of 0.52–1.24 nm, which can filter out the dissolved polysulfide species (1.0–1.8 nm). Also, SWCNTs possess a specific surface area of 527 $m^2 g^{-1}$ which provides a more accessible reaction area for reactivating the trapped active materials. Benefiting from these advantages, the SWCNT-modulated separator resulted in a Li–S cell with a small capacity fading rate of only 0.18% per cycle over 300 cycles at C/5 in an electrolyte of 1.85 M $LiCF_3SO_3$ and 0.1 M $LiNO_3$ in DOL/DME (1 : 1, v : v), much lower than that (1.3% per cycle) of a pristine Celgard separator. More recently, scaled-up fabrication of porous-graphene-modified separators was reported.[152] The fabrication of porous-graphene-modified separators was readily scaled-up for assembling and evaluating Li–S pouch cells with a large areal sulfur loading of 7.8 mg cm^{-2} and the initial discharge capacity was 1135 mA h g^{-1} at a current density of 0.1C in an electrolyte of 1 M LiTFSI and 1 wt% $LiNO_3$ in DOL/DME (1 : 1, v : v).

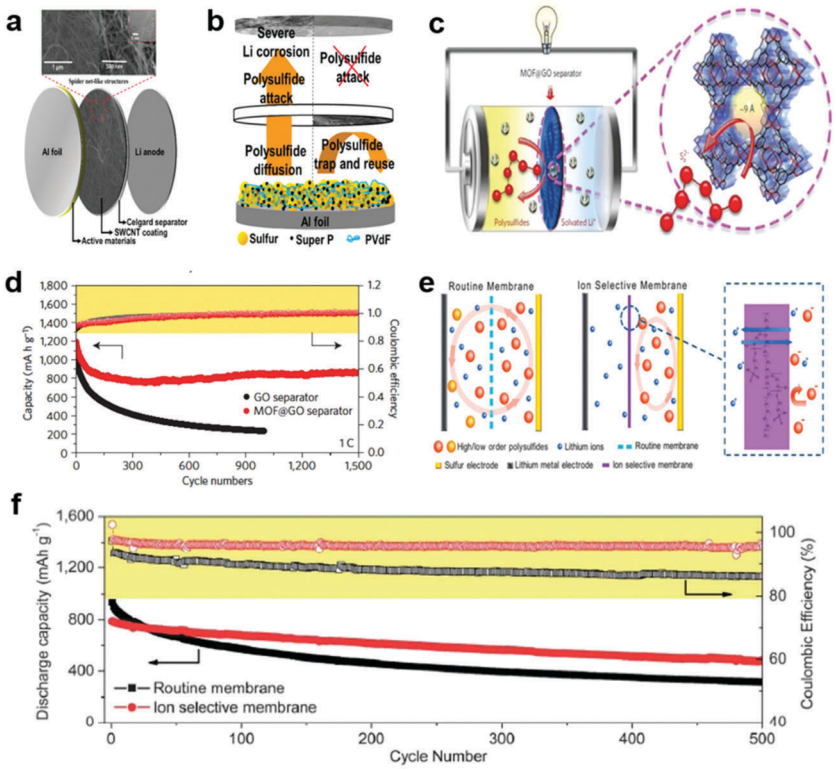

Fig. 5 Li–S batteries with functionalized polyolefin-based separators. (a) Schematic and SEM images of the spider net-like SWCNT-modulated separator configuration, and (b) the improvement mechanism of the SWCNT-modulated separator. Reprinted with permission from ref. 129. Copyright 2016, Wiley-VCH. (c) Schematic of metal–organic framework@graphene oxide (MOF@GO) separators in Li–S batteries. The enlarged image illustrates the MOF pore size (approximately 9 Å), which is significantly smaller than that of the polysulfides (Li_2S_n, $4 < n \leq 8$). (d) Cycling performance at a rate of 1C over 1500 cycles with MOF@GO separators and over 1000 cycles with GO separators. Reprinted with permission from ref. 138. Copyright 2016, Nature Publishing Group. (e) Schematic of a Li–S cell with ion selective membranes, in which the polysulfide anions are limited to the cathode side, (f) the change in discharge capacities and coulombic efficiency *vs.* the cycle number at a current density of 1C. Reprinted with permission from ref. 147. Copyright 2014, Royal Society of Chemistry.

3.1.2 Metal oxide modified polyolefin separators. To suppress the shuttle effect in Li–S batteries, various metal oxides are extensively utilized for separator modification, owing to their strong binding interactions with polysulfides besides the physical confinement, as well as their facile synthesis with low cost. Until now, many metal oxides have been proved to be effective for modifying the separator, such as Al_2O_3,[135] TiO_2,[136] RuO_2,[137] *etc.* For example, Li *et al.* demonstrated an Al_2O_3-coated separator with developed porous channels for blocking polysulfide migrations.[135] The Al_2O_3-coating layer with excellent stability was shown to be very effective in suppressing the shuttle effect, resulting in decreased capacity decay with a high reversible capacity of 593.4 mA h g^{-1} over 50 cycles in the electrolyte of 1.5 M LiTFSI and 0.3 M $LiNO_3$ in DOL/DME (1 : 1, v : v). Giebeler *et al.* developed a novel RuO_2 nanoparticle-embedded mesoporous carbon-coated separator that utilizes a catalytic oxide for facilitating the trapping and redox reaction of polysulfide.[137] The RuO_2–carbon hybrids showed high adsorption ability of polysulfide and enable the reutilization of the adsorbed polysulfide owing to the catalytic feature of RuO_2 nanoparticles, thus leading to effective stabilization and better utilization of the sulfur cathode. Zhou *et al.* reported a metal–organic framework (MOF)-based separator that functions as an efficient ionic sieve towards polysulfides diffusing to the anode with a negligible effect on the transfer of lithium ions (Fig. 5c).[138] The chosen $Cu_3(BTC)_2$ MOF materials possess highly ordered micropores with a size window of about 9 Å, which are much smaller than the diameters of lithium polysulfide (Li_2S_n, $4 < n \leq 8$), thus making them excellent candidates as ionic sieves to mitigate the polysulfides. As a result, the cell with this MOF-based separator exhibited a low capacity decay rate (0.019% per cycle over 1500 cycles) (Fig. 5d). Kim *et al.* presented a separator coated with poled barium titanium oxide ($BaTiO_3$) that can form permanent dipoles upon an electric field, which were found to be effective for preventing polysulfide from migrating across the separator through electrostatic repulsion.[139] The ferroelectric character of $BaTiO_3$ can align the dipoles in $BaTiO_3$ particles and render the dipoles permanently polarized even after the electric potential is shut off. Besides, the $BaTiO_3$-based separator can greatly restrain thermal shrinkage of the polyethylene separator at high temperatures, thus enhancing the safety of the cell. As a consequence, the Li–S cell with the $BaTiO_3$-based separator greatly improved the cycling performance with 82.8% retention after 50 cycles.

3.1.3 Polymer modified polyolefin separators. Polymer modified separators are another effective strategy for separator

modification to mitigate the shuttling behavior of polysulfides. The polymer-based separators are usually light-weight, with hierarchically porous structures and functional groups (oxygen-, nitrogen-, and sulfur-doped atoms, *etc.*), which are advantageous for improving the efficiency of trapping the polysulfides in Li–S batteries. For instance, Wei *et al.* reported an ion selective membrane fabricated by a Nafion-coated Celgard separator, which can act as an electrostatic shield for polysulfide anions (Fig. 5e).[147] The SO^{3-} groups of Nafion can block the diffusion of negative polysulfide anions (S_n^{2-}) while allowing the transfer of positive lithium ions. In this case, lithium ions transfer freely and no significant increase in polarization and electrochemical impedance is detected in the cell with the ion selective separator. The resulting cell with this separator exhibited significantly improved cycling performance with an ultralow decay rate of 0.08% per cycle over 500 cycles with an electrolyte without $LiNO_3$, which was less than half that of the pristine membranes (Fig. 5f). Similarly, Liu *et al.* prepared a polydopamine modified separator with a hydrophilic surface to suppress polysulfide transportation and improve the performance of Li–S batteries.[148] Compared with the bare hydrophobic separator, the polydopamine layer can better trap the polysulfide migrating towards the anode, maintain the electron conductivity of the electrode after discharge and ensure fast transport of electrons from the electrode to the deposited Li_2S during the charge process, thus enhancing the gradual reactivation of Li_2S. The cells with the hydrophilic polydopamine-modified separator exhibited enhanced cycle performance with much higher retention of capacity than the cells using conventional separators. Wu *et al.* reported a modification of separators with conductive polymers for enhancing the cycling performance of Li–S batteries.[149] In particular, a polypyrrole-modified separator was fabricated, which possessed strong binding interactions with polysulfides, and good electronic and ionic conductivity. The polypyrrole can mitigate the diffusion of polysulfides in the electrolyte and decrease the polarization of the sulfur cathode, resulting in enhanced performance. As a result, the Li–S batteries with the polypyrrole-modified separator showed a good capacity retention of 801.6 mA h g^{-1} over 300 cycles at 0.5C, with its Columbic efficiency up to 90.6% in a $LiNO_3$-free electrolyte.

In addition to the above-mentioned material modified separators, multi-component modifications, *e.g.* carbon/polymer or carbon/metal oxide hybrid materials, have been investigated to produce composite separators with multi-functions. Multi-component coating layers such as mesoporous carbon/polyethylene glycol (PEG),[153] CNT/PEG,[154] C/PVDF,[155] CNT/polyaniline nanofiber,[156] graphene oxide/Nafion,[157] CNT/Al_2O_3,[158] and nitrogen-doped graphene/nickel–iron layered double hydroxides,[159] which combine the advantage of high conductivity of carbon materials with high trapping capability for polysulfides of polymers/metal oxides, have shown great potential to improve the rate and cycling performance of Li–S batteries.

The progresses in functionalized separators open up a new direction towards high-performance Li–S cells. The separators could be modified by electrically conductive materials, which act as an upper current collector to improve the electrochemical performance of cathode materials, or ion selective polymer or metal oxides, which can inhibit the diffusion of polysulfides by either physical confinement or chemical interactions. Multi-functional separators are effective to improve Li–S cells or even other battery systems with high-rate performance and long cycle life.

3.2 Functionalized novel material-based separators

The polyolefin, such as polyethylene and polypropylene, based separators have been commercialized in lithium ion batteries and widely applied in Li–S batteries, due to their excellent stable electrochemical properties and excellent mechanical strength. However, the inherent drawbacks of these polyolefin separators such as low porosity, poor electrolyte wettability and thermal stability, especially the enormous shrinkage at elevated temperatures, have hindered their further applications in advanced batteries. Therefore, it is necessary to design and fabricate novel separators with improved features for applications in high-performance Li–S batteries. Recently, non-polyolefin based polymers such as Nafion,[160,161] PAN,[162] and inorganic ceramics[163–167] have been studied and applied as separators for Li–S batteries.

Nafion ionomer film, a copolymer of tetrafluoroethylene and perfluoro vinyl ether, is well-known for its excellent stability, high cationic conductivity and unity transference number. As a result, a thick lithiated Nafion ionomer film (50 μm) was directly used as a functional separator for Li–S cells.[160] The $-SO^{3-}$ groups in Nafion channels allow the positively charged Li^+ to freely diffuse through the separator, whereas the movement of the negatively charged polysulfide was inhibited due to the electrostatic repulsion. The improvement in cycle performance and coulombic efficiency was due to the inhibited transport of polysulfide anions through the ionomer film, which helped to decrease the loss of active mass and the corrosion of the Li electrode, and inhibit the shuttle phenomenon. Manthiram and his co-workers further improved the cell structure by using a lithiated Nafion membrane as a separator and a high-surface activated carbon nanofiber as a cathodic interlayer for Li–S batteries.[161] The Li–S battery system with the lithiated Nafion membrane and the sandwiched cathode exhibited significantly enhanced cyclability relative to the cells with the traditional liquid-electrolyte integrated porous separator. However, the voltage (*vs.* Li/Li^+) of the second discharge plateau for the cell was dramatically reduced from 2.1 V to 1.9 V, evidencing a high ion transport resistance caused by the Nafion membrane thickness. At the same time, the Nafion film increased the polarization, which eventually degraded the energy efficiency of the battery. The combinations between the Nafion monomer films and other membranes may alleviate these drawbacks. PAN has high electrochemical performance due to the dipole interactions between nitrile groups in PAN and Li^+ in the electrolytes. The PAN separators can also reduce the sizes of lithium dendrites owing to the viscoelastic polymer by mechanically suppressing the dendrite formation. Zhu *et al.* made a highly porous PAN/graphene oxide nanofiber membrane for Li–S batteries.[162] The schematic model and mechanism of inhibiting polysulfide diffusion of the separator are shown in Fig. 6a. Due to high energy binding between nitrile groups and Li_2S/polysulfides

and the electrostatic interactions between GO and negatively charged species (S_n^{2-}), the PAN/graphene oxide separator can effectively block the polysulfide migration and further enhance the utilization of the active material. The highly porous structure of the membrane made the separator have excellent electrolyte wettability, high ionic conductivity, and rapid ionic transportation. After 100 cycles, the cell with a PAN/GO separator can still deliver a high capacity of 597 mA h g^{-1} in the electrolyte of 1 M LiTFSI and 1 wt% $LiNO_3$ in DOL/DME (1 : 1, v : v), which is 38% higher than that of the cell with a polypropylene separator (Fig. 6b). In addition, a low capacity retention loss (5%) could be achieved even after a resting time of 24 h, indicating the excellent anti-self-discharge capability of the PAN/graphene oxide nanofiber membrane.

In addition to organic polymer-based separators, glass fiber membranes have received attention because they have a highly porous structure, excellent electrolyte wettability, and superior thermal stability, which makes them quite suitable for application as a separator in Li–S batteries. It has been reported that a glass fiber membrane could lead to large electrolyte intake and consequently high ionic conductivity when placed in the electrolyte, facilitating rapid ionic transportation. In 2015, a hybrid separator composed of a glass fiber membrane and Celgard microporous PP/PE membrane was developed for Li–S batteries by Xia and coworkers.[163] Their results showed that the cell with this hybrid separator in DOL/DME (1 : 1, v : v) containing 1 M LiTFSI delivered a specific capacity of 1050 mA h g^{-1} at the 10th cycle with a current density of 0.2C, which was significantly higher than that (450 mA h g^{-1}) achieved by the cell with the Celgard membrane. However, the use of hybrid separators would decrease the gravimetric and volumetric energy density of the cells, as well as increase the resistance of the cell. In this regard, the direct use of glass fiber as the separator for Li–S batteries has been reported.[164] It was shown that glass fiber could increase the intake of soluble polysulfide intermediates, thus preventing the diffusion of the intermediates to the Li anode. Moreover, the membrane had intrinsic thermal resistance due to the borosilicate structure. All of these factors provided a high retention capacity of 617 mA h g^{-1} after 100 cycles at a current density of 0.2C with 1 M LiTFSI and 0.1 M $LiNO_3$ in DOL/DME (1 : 1, v : v) as an electrolyte. A possible concern for the direct application of glass fiber in Li–S batteries is the poor flexibility of the glass fiber material. Coating the glass fiber separator with a conductive carbon layer further improves the battery performance.[165] The carbon layer not only acts as a barrier to inhibit the diffusion of soluble polysulfide species at a high S loading of 70% but also reduces the cell resistance and serves as a second current collector for S (Fig. 6c). A Li–S battery with the carbon-coated glass fiber separator showed an initial discharge capacity of 1352 mA h g^{-1} at 0.2C and a columbic efficiency of 97.6% after 200 cycles (Fig. 6d), as well as

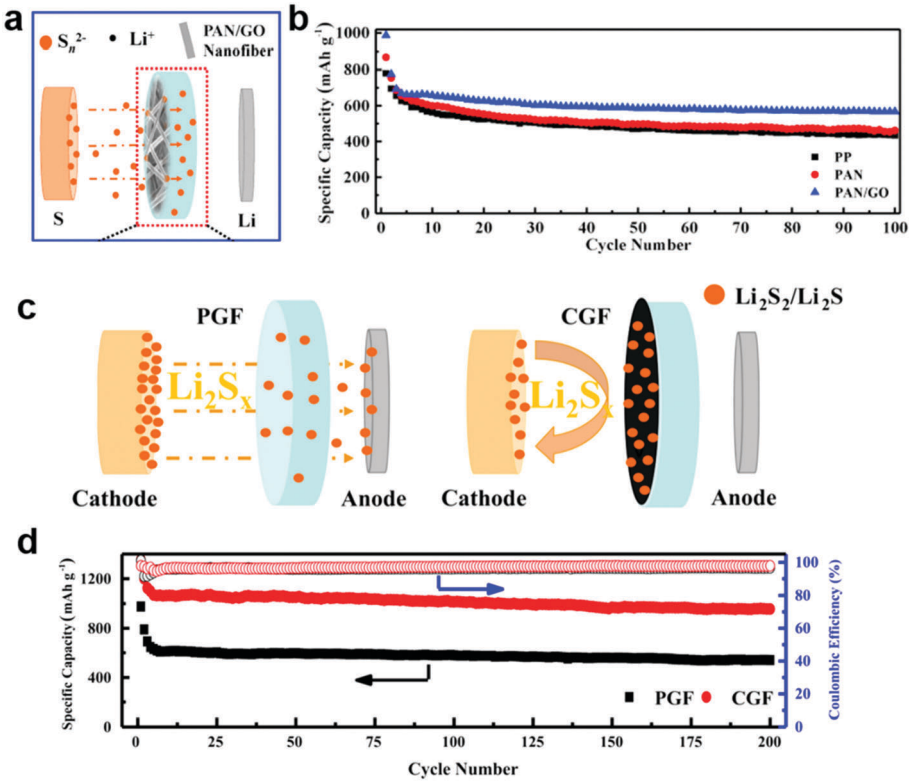

Fig. 6 Li–S batteries with functionalized novel material-based separators. (a) Schematic illustration of the Li–S cell with a PAN/GO separator. (b) Cycling performance of Li–S cells with polypropylene (PP), PAN, and PAN/GO separators at a current density of 0.2C. Reprinted with permission from ref. 162. Copyright 2016, Elsevier. (c) Schematic of polysulfide diffusion in Li–S cells with pristine glass fiber (PGF, left) and carbon-coated glass fiber (CGF, right) during discharge. (d) Cycling performance of Li–S cells with PGF and CGF at a current density of 0.2C. Reprinted with permission from ref. 165. Copyright 2016, Elsevier.

good high-rate response up to 4C with 1 M LiTFSI and 0.1 M $LiNO_3$ in DOL/DME (1 : 1, v : v) as an electrolyte. In addition to carbon, other organic macromolecules such as melamine formaldehyde,[168] graphitic carbon nitride (g-C_3N_4),[169] and few-layered Ti_3C_2 nanosheets[170] have been introduced for modification of the glass fiber membrane to fabricate functional separators for Li–S batteries. These coatings can either improve the thermal stability of the separators at elevated temperatures, enhance the adsorption capacity for polysulfides, or decrease the internal resistance of the cell.

Much progress has been made in the search for alternatives to polyolefin separators. Both non-polyolefin polymeric separators and ceramic separators have been reported to be potential candidates for applications in Li–S batteries. However, there are inherent limitations for practical application of separators based on new materials. For example, functional polymeric separators such as Nafion improve the cell performance by the inhibition of polysulfide shuttling, while the extra resistance for lithium ions is inevitable. Therefore, a reasonable balance between the polysulfide blocking efficiency and lithium ion flux as well as the separator thickness and safety concerns should be taken into consideration. For inorganic ceramic separators, a possible concern is the poor mechanical stability despite their superior thermal stability. Therefore, for future studies, significant efforts should be devoted to further improving the performance of these separators and understanding the relationship between their properties and battery performance.

4 Interlayers in a sandwiched/integrated structure

A Li–S battery is an integrated device, involving not only materials, but also electrode architecture and cell engineering, for which the energy density is one of the most important parameters. Despite the considerable research that has been conducted on the material design for the electrode, especially the cathode, more and more attention has been paid to the electrode architecture and cell engineering. Design parameters, including the areal sulfur loading and ratio of active to inactive components, should be taken into consideration since they play a key role in determining the useful energy density of the Li–S cells. In order to achieve a high specific energy for Li–S batteries for practical applications, the sulfur content and areal sulfur loading in the cathode should be as high as possible, while the weight of inactive components in the cell (*e.g.*, current collectors, electrolytes) needs to be as low as possible.[2,171] Although inserting an interlayer or modifying the separator could effectively inhibit the polysulfide migration, the introduction of secondary barrier layers increases the weight of inactive components and amount of electrolyte, as well as blocks Li^+ diffusion to some extent due to the increased thickness. Therefore, the secondary barrier layers should be thin enough to guarantee fast ion diffusion through it and reduce the unnecessary weight to enhance the energy density of the whole cell. Hence, designing the interlayer into a sandwiched/integrated structure can reduce unnecessary weight and possess higher areal sulfur mass loading with enhanced specific energy, which are currently essential for further enhancement of the electrochemical performance of Li–S batteries. In this section, some advanced examples of introducing interlayers with a sandwiched/integrated structure for novel structural configurations for Li–S batteries, are presented and discussed.

In general, a battery mainly consists of two electrodes: a cathode and an anode, separated by a polymer separator. If S/lithium polysulfides can be confined in the cathode side and be efficiently reused during cycling, the cycling stability and rate capability of the Li–S battery will be improved. With these considerations, a unique sandwiched structure was designed with pure sulfur sandwiched between two carbon layers. The sandwiched structure can be fabricated from either assembly of separated membranes[172] or integrated flexible architectures by doctor-blading[173,174] or vacuum filtration techniques.[175] Cheng *et al.* reported a unique sandwich structure with pure sulfur between two graphene membranes.[172] One graphene membrane was used as a current collector (GCC) with sulfur coated on it as the active material, and the other graphene membrane was coated on a commercial polymer separator (G-separator) (denoted as GCC/S + G-separator, as illustrated in Fig. 7a and b). When the discharge current density was increased to 1.5 and 6 A g^{-1}, the battery with a GCC/S + G-separator still delivered capacities as high as 1000 and 750 mA h g^{-1}, respectively, which are 2 and 50 times higher than those of the battery with Al foil/S + separator tested under the same conditions. The sulfur electrode exhibited good long-term cycling stability and retained a capacity of 680 mA h g^{-1} at a current density of 1.5 A g^{-1} for 300 cycles with a Columbic efficiency above 97% in DOL/DME (1 : 1, v : v) with 1 M LiTFSI and 0.5 wt% $LiNO_3$, and the capacity decay was only 0.1% per cycle (Fig. 7c). Moreover, a free-standing integrated cathode with a sandwiched structure was synthesized using a three-step vacuum-assisted filtration method.[175] First, the thin carbonaceous bottom layer was prepared by filtration of carbon nanotube/nanofibrillated cellulose (CNT/NFC) solution, followed by ultrasonicating a dispersed solution containing nitrogen-doped graphene/sulfur and CNT/NFC, then filtering to form the middle active layer. Finally, the upper thin carbonaceous layer was prepared the same as in the first step. Interconnected CNT/NFC layers on both sides of the active layer can entrap polysulfide species and supply efficient electron transport. In particular, the electrode with a high areal sulfur loading of 8.1 mg cm^{-2} exhibited an areal capacity of $\sim$8 mA h cm^{-2} and an ultralow capacity fading of 0.067% per cycle over 1000 discharge/charge cycles at C/2 rate in DOL/DME (1 : 1, v : v) with 1 M LiTFSI and 2 wt% $LiNO_3$, while the average Columbic efficiency is around 97.3%, indicating good electrochemical reversibility. Guo *et al.* further designed an integrated flexible cathode architecture consisting of a carbon/sulfur/carbon sandwiched structure spread directly on a polypropylene separator (CSC@separator) using the simple doctor-blading technique.[173] Commercial sulfur and Super P carbon were used as raw materials to be coated on the polypropylene separator as the sulfur layer and carbon layer, respectively. An illustration of the cell configuration using a

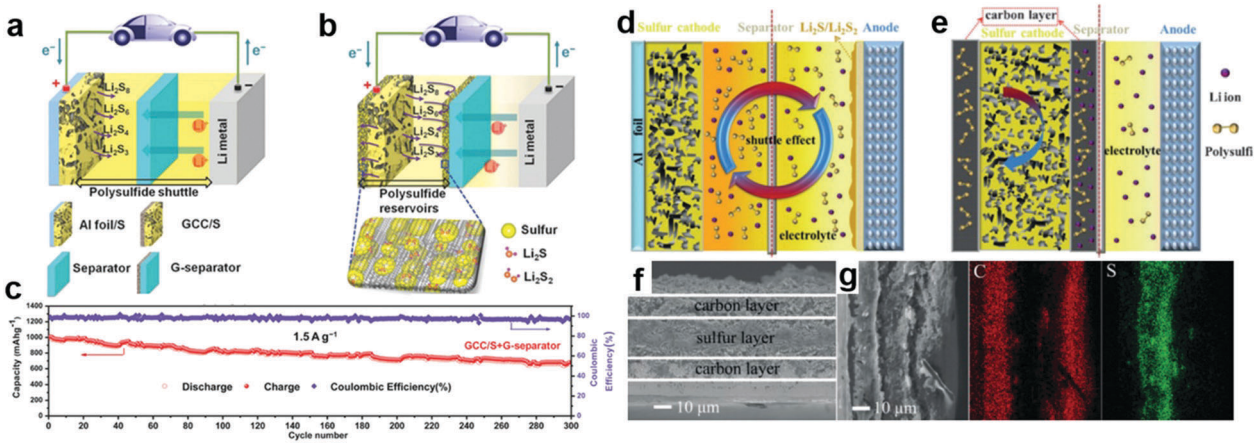

Fig. 7 Schematic of a Li–S battery with (a) the conventional electrode configuration: Al foil/S + separator, and (b) a sandwiched electrode configuration: graphene current collector (GCC), sulfur cathode, and graphene coated separator (GCC/S + G-separator). (c) Cycling stability of the Li–S batteries with the GCC/S + G-separator at 1.5 A g^{-1} for 300 cycles. Reprinted with permission from ref. 172. Copyright 2014, Wiley-VCH. Illustration of Li–S cell configurations employing (d) conventional electrodes and (e) carbon/sulfur/carbon (CSC) integrated sandwich-structured electrodes. (f) Cross-section of the CSC@separator electrode and (g) corresponding elemental mapping. Reprinted with permission from ref. 173. Copyright 2016, Wiley-VCH.

conventional electrode and the CSC@separator electrode is shown in Fig. 7d and e. The CSC sandwiched layers are directly coated on the separator without using Al foil as a substrate, greatly reducing the weight of the electrode (the weight of the substrate is reduced by 78%) and exhibits excellent flexibility. The layered carbon/sulfur/carbon sandwich structure is clearly confirmed by cross-sectional scanning electron microscope image and elemental mapping results (Fig. 7f and g). The CSC@separator electrode exhibited good long-term cycling stability with the capacity stabilized around 730 mA h g^{-1} at 0.6C after 500 cycles in DOL/DME (1 : 1, v : v) with 1 M LiTFSI and 2 wt% $LiNO_3$, corresponding to 71.2% capacity retention and a small capacity fading of only 0.058% per cycle.

These carbon/sulfur/carbon sandwiched structures exhibit several distinguished advantages listed as follows: (1) the two carbon layers on both sides of the sulfur electrode provide excellent electrical conductivity, acting as double current collectors from top to bottom to accelerate electron transport into the active material. (2) The sandwiched structure can accommodate the large volumetric expansion of sulfur during lithiation, preventing pulverization of the active material and maintaining the integrity of the whole electrode. (3) The double carbon layers can act as sulfur reservoirs during cycling when part of the sulfur migrates inside the carbon membranes. (4) The carbon layer beside the separator would block the migration of polysulfides from the S cathode to the Li anode, resulting in suppression of the shuttling effect and improved long-term cycling stability. (5) Because the density of carbon is only one quarter of that of an Al-foil current collector, the bottom carbon layer replacing the traditional Al-foil current collector can further improve the specific energy density when assembled into a battery. (6) Furthermore, the surface roughness of carbon materials can improve the adhesion of sulfur to it and lower the impedance and polarization of the Li–S batteries. Therefore, compared to the conventional Li–S battery configuration, these properties provide the newly designed Li–S batteries with long cycling life and excellent rate performance. In addition, this design avoids any surface modification of sulfur particles and simplifies the fabrication of sulfur cathodes, giving it strong potential for the industrial production and application of Li–S batteries.

5 Summary and outlook

In summary, we have reviewed the recent developments of innovative configurations in Li–S batteries in the past several years, including cathodic interlayers, separator modification and interlayers with sandwiched/integrated structures, mainly focusing on the strategies and resultant performance of Li–S batteries. Inserting an interlayer between the separator and S cathode is found to be effective in inhibiting the migration of the polysulfides from the sulfur electrode in Li–S batteries. The multifunctional modified separators are beneficial in avoiding the formation of lithium dendrites and promoting a long cycling life. Notably, either being an individual layer or a thin coating on the cathode and separator, these secondary barrier layers are proved to be effective for mitigating the shuttling behavior. Nonpolar carbon acts only as a physical barrier to polysulfide migration due to its weak interaction with polysulfides, while metal oxides/sulfides can capture the polysulfides more effectively due to a strong chemical interaction, but their low electrical conductivity hinders the reuse of these captured sulfur species. Therefore, there is a tendency to make a hybrid interlayer by compounding metal oxides/sulfides with highly conductive carbon for stronger interaction with polysulfides as well as fast electron transfer inside the cathode.

While developing advanced barrier layers contributes to improved electrochemical performance, several issues should be addressed. First, the secondary barrier layers should cut down the direct contact of sulfur with the bulk electrolyte and effectively block the diffusion of the polysulfides, so a compact coating on the cathode is ideal for this purpose by confining

polysulfides inside it. Second, the introduction of secondary barrier layers increases the weight of inactive components and leads to a decreased sulfur content based on the whole cathode, as well as unexpectedly blocks Li ion diffusion to some extent because of their large thickness. Therefore, the secondary barrier layers should be thin enough to guarantee fast ion diffusion through it and reduce the unnecessary weight to enhance the energy density of the whole cell. Thus, a well manipulated approach is needed for preparation of the ultra-thin coating. Meanwhile, the extra coating layer or interlayer in the system inevitably increases the electrolyte uptake, which also has a negative effect on the gravimetric and volumetric energy density of the Li–S cells. Nevertheless, for most studies, the reported electrolyte/sulfur ratios are often much higher than should be used in a practical Li–S batteries to ensure a high energy density (less than or equal to 4 $\mu L\ mg^{-1}$). Therefore, more work needs to be done to improve the electrochemical performance and energy density of Li–S batteries with the use of small amounts of electrolyte. Third, the secondary barrier layers must be robust and conductive so that they can act as an upper current collector, where the captured polysulfides inside the secondary barrier layers can be reused effectively. Moreover, in order to achieve a high specific energy for Li–S batteries for practical applications, more attention should be paid to cell engineering, with high sulfur loading and scalable fabrication approaches taken into consideration. Thus, integrated cell configurations may be an alternative solution since they combine several advantages such as lightweight, good conductivity, efficient polysulfide reservoir, and mechanical flexibility. Therefore, compared to the conventional Li–S battery configuration, these properties provide the newly designed Li–S batteries with long cycling life and excellent rate performance. In addition, emerging research interests have also been focused on soft-package Li–S batteries and their real application, which is an inevitable tendency for the development of Li–S batteries.

Conflicts of interest

There are no conflicts to declare.

Acknowledgements

The authors are grateful for the financial support from the National Natural Science Foundation of China (51433001 and 21704014), the China Postdoctoral Science Foundation (2016M601471), the Shanghai Sailing Program (17YF1400200), and the Fundamental Research Funds for the Central Universities.

Notes and references

1 A. Manthiram, Y. Z. Fu, S. H. Chung, C. X. Zu and Y. S. Su, *Chem. Rev.*, 2014, **114**, 11751–11787.
2 R. P. Fang, S. Y. Zhao, Z. H. Sun, D. W. Wang, H. M. Cheng and F. Li, *Adv. Mater.*, 2017, **29**, 1606823.
3 Y. Zheng, T. Zhou, X. Zhao, W. K. Pang, H. Gao, S. Li, Z. Zhou, H. K. Liu and Z. P. Guo, *Adv. Mater.*, 2017, **29**, 1700396.
4 L. Mei, J. T. Xu, Z. X. Wei, H. K. Liu, Y. T. Li, J. M. Ma and S. X. Dou, *Small*, 2017, 1701441.
5 L. S. Zhang, W. Fan and T. X. Liu, *Nanoscale*, 2016, **8**, 16387–16394.
6 Y. E. Miao, Y. P. Huang, L. S. Zhang, W. Fan, F. L. Lai and T. X. Liu, *Nanoscale*, 2015, **7**, 11093–11101.
7 K. Cao, L. Jiao, H. Liu, Y. Liu, Y. Wang, Z. Guo and H. Yuan, *Adv. Energy Mater.*, 2015, **5**, 1401421.
8 L. S. Zhang, Y. P. Huang, Y. F. Zhang, W. Fan and T. X. Liu, *ACS Appl. Mater. Interfaces*, 2015, **7**, 27823–27830.
9 W. Q. Li, Q. Wang, K. Cao, J. J. Tang, H. T. Wang, L. M. Zhou and H. M. Yao, *Compos. Commun.*, 2016, **1**, 1–5.
10 H. Li, L. Xu, H. Sitinamaluwa, K. Wasalathilake and C. Yan, *Compos. Commun.*, 2016, **1**, 48–53.
11 P. G. Bruce, S. A. Freunberger, L. J. Hardwick and J. Tarascon, *Nat. Mater.*, 2011, **11**, 19–29.
12 Y. X. Yin, S. Xin, Y. G. Guo and L. J. Wan, *Angew. Chem., Int. Ed.*, 2013, **52**, 13186–13200.
13 L. Ma, K. E. Hendrickson, S. Wei and L. A. Archer, *Nano Today*, 2015, **10**, 315–338.
14 H. Q. Wang, V. Sencadas, G. P. Gao, H. Gao, A. J. Du, H. K. Liu and Z. P. Guo, *Nano Energy*, 2016, **26**, 722–728.
15 X. Fang and H. S. Peng, *Small*, 2015, **11**, 1488–1511.
16 Z. W. Seh, Y. Sun, Q. Zhang and Y. Cui, *Chem. Soc. Rev.*, 2016, **45**, 5605–5634.
17 X. Ji, S. Evers, R. Black and L. F. Nazar, *Nat. Commun.*, 2011, **2**, 325.
18 J. Lochala, D. Y. Liu, B. B. Wu, C. Robinson and J. Xiao, *ACS Appl. Mater. Interfaces*, 2017, **9**, 24407–24421.
19 S. Rehman, K. Khan, Y. F. Zhao and Y. L. Hou, *J. Mater. Chem. A*, 2017, **5**, 3014–3038.
20 L. Qie, C. Zu and A. Manthiram, *Adv. Energy Mater.*, 2016, **6**, 1502459.
21 H. Q. Wang, C. F. Zhang, Z. Chen, H. K. Liu and Z. P. Guo, *Carbon*, 2015, **81**, 782–787.
22 X. Ji and L. F. Nazar, *J. Mater. Chem.*, 2010, **20**, 9821–9826.
23 J. Scheers, S. Fantini and P. Johansson, *J. Power Sources*, 2014, **255**, 204–218.
24 Y. Yang, G. Zheng and Y. Cui, *Chem. Soc. Rev.*, 2013, **42**, 3018–3032.
25 M. A. Pope and I. A. Aksay, *Adv. Energy Mater.*, 2015, **5**, 1500124.
26 Z. Li, Y. M. Huang, L. X. Yuan, Z. X. Hao and Y. H. Huang, *Carbon*, 2015, **92**, 41–63.
27 J. Ni, S. Fu, C. Wu, J. Maier, Y. Yu and L. Li, *Adv. Mater.*, 2016, **28**, 2259–2265.
28 Y. Ding, P. Kopold, K. Hahn, P. A. van Aken, J. Maier and Y. Yu, *Adv. Funct. Mater.*, 2016, **26**, 1112–1119.
29 M. K. Liu, Y. Q. Liu, Y. Yan, F. S. Wang, J. H. Liu and T. X. Liu, *Chem. Commun.*, 2017, **53**, 9097–9100.
30 A. Hoefling, D. T. Nguyen, Y. J. Lee, S. Song and P. Theato, *Mater. Chem. Front.*, 2017, **1**, 1818–1822.
31 X. Liu, J. Huang, Q. Zhang and L. Q. Mai, *Adv. Mater.*, 2017, **29**, 1601759.

32 X. Chen, Z. B. Xiao, X. T. Ning, Z. Liu, Z. Yang, C. Zou, S. Wang, X. H. Chen, Y. Chen and S. M. Huang, *Adv. Energy Mater.*, 2014, **4**, 1301988.
33 C. Tang, Q. Zhang, M. Q. Zhao, J. Q. Huang, X. B. Cheng, G. L. Tian, H. J. Peng and F. Wei, *Adv. Mater.*, 2014, **26**, 6100–6105.
34 Q. Li, Z. Zhang, Z. Guo, K. Zhang, Y. Lai and J. Li, *J. Power Sources*, 2015, **274**, 338–344.
35 C. F. Zhang, H. B. Wu, C. Z. Yuan, Z. P. Guo and X. W. D. Lou, *Angew. Chem., Int. Ed.*, 2012, **51**, 9592–9595.
36 N. Jayaprakash, J. Shen, S. S. Moganty, A. Corona and L. A. Archer, *Angew. Chem., Int. Ed.*, 2011, **50**, 5904–5908.
37 X. Ji, K. T. Lee and L. F. Nazar, *Nat. Mater.*, 2009, **8**, 500–506.
38 O. Ogoke, G. Wu, X. Wang, A. Casimir, L. Ma, T. Wu and J. Lu, *J. Mater. Chem. A*, 2017, **5**, 448–469.
39 M. Liu, X. Y. Qin, Y. B. He, B. H. Li and F. Y. Kang, *J. Mater. Chem. A*, 2017, **5**, 5222–5234.
40 J. T. Xu, J. M. Ma, Q. H. Fan, S. J. Guo and S. X. Dou, *Adv. Mater.*, 2017, **29**, 1606454.
41 S. Zhang, K. Ueno, K. Dokko and M. Watanabe, *Adv. Energy Mater.*, 2015, **5**, 1500117.
42 R. Cao, W. Xu, D. Lv, J. Xiao and J. Zhang, *Adv. Energy Mater.*, 2015, **5**, 1402273.
43 J. Y. Li, Q. Xu, G. Li, Y. X. Yin, L. J. Wan and Y. G. Guo, *Mater. Chem. Front.*, 2017, **1**, 1691–1708.
44 T. Tao, S. G. Lu, Y. Fan, W. W. Lei, S. M. Huang and Y. Chen, *Adv. Mater.*, 2017, **29**, 1700542.
45 Y. Su and A. Manthiram, *Nat. Commun.*, 2012, **3**, 1166.
46 J. Hwang, H. M. Kim, S. Lee, J. Lee, A. Abouimrane, M. A. Khaleel, I. Belharouak, A. Manthiram and Y. K. Sun, *Adv. Energy Mater.*, 2016, **6**, 1501480.
47 H. M. Kim, H. Sun, I. Belharouak, A. Manthiram and Y. Sun, *ACS Energy Lett.*, 2016, **1**, 136–141.
48 Y. Su and A. Manthiram, *Chem. Commun.*, 2012, **48**, 8817–8819.
49 C. Lee and I. Kim, *Nanoscale*, 2015, **7**, 10362–10367.
50 H. M. Kim, J. Hwang, A. Manthiram and Y. Sun, *ACS Appl. Mater. Interfaces*, 2016, **8**, 983–987.
51 M. Li, W. Wahyudi, P. Kumar, F. Wu, X. Yang, H. Li, L. Li and J. Ming, *ACS Appl. Mater. Interfaces*, 2017, **9**, 8047–8054.
52 C. Zu, Y. Su, Y. Fu and A. Manthiram, *Phys. Chem. Chem. Phys.*, 2013, **15**, 2291–2297.
53 X. Wang, Z. Wang and L. Chen, *J. Power Sources*, 2013, **242**, 65–69.
54 Q. R. Zeng, X. Leng, K. Wu, I. R. Gentle and D. Wang, *Carbon*, 2015, **93**, 611–619.
55 J. Huang, Z. Xu, S. Abouali, M. Akbari Garakani and J. Kim, *Carbon*, 2016, **99**, 624–632.
56 M. Shaibani, A. Akbari, P. Sheath, C. D. Easton, P. C. Banerjee, K. Konstas, A. Fakhfouri, M. Barghamadi, M. M. Musameh, A. S. Best, T. Rüther, P. J. Mahon, M. R. Hill, A. F. Hollenkamp and M. Majumder, *ACS Nano*, 2016, **10**, 7768–7779.
57 S. Chung and A. Manthiram, *Adv. Mater.*, 2014, **26**, 1360–1365.
58 S. Chung and A. Manthiram, *Chem. Commun.*, 2014, **50**, 4184–4187.
59 Z. X. Cao, C. Ma, Y. H. Yin, J. Zhang, Y. M. Ding, M. J. Shi and S. T. Yang, *New J. Chem.*, 2015, **39**, 9659–9664.
60 R. Singhal, S. Chung, A. Manthiram and V. Kalra, *J. Mater. Chem. A*, 2015, **3**, 4530–4538.
61 J. G. Wang, Y. Yang and F. Y. Kang, *Electrochim. Acta*, 2015, **168**, 271–276.
62 S. Choi, J. J. Song, C. Y. Wang, S. Park and G. X. Wang, *Chem. – Asian J.*, 2017, **12**, 1470–1474.
63 D. K. Lee, C. W. Ahn and H. Jeon, *J. Power Sources*, 2017, **360**, 559–568.
64 T. Gao, T. Le, Y. Yang, Z. Yu, Z. Huang and F. Y. Kang, *Materials*, 2017, **10**, 376.
65 Y. Huang, M. Zheng, Z. Lin, B. Zhao, S. Zhang, J. Yang, C. Zhu, H. Zhang, D. Sun and Y. Shi, *J. Mater. Chem. A*, 2015, **3**, 10910–10918.
66 S. Li, G. Ren, M. N. F. Hoque, Z. Dong, J. Warzywoda and Z. Fan, *Appl. Surf. Sci.*, 2017, **396**, 637–643.
67 J. Balach, T. Jaumann, M. Klose, S. Oswald, J. Eckert and L. Giebeler, *J. Phys. Chem. C*, 2015, **119**, 4580–4587.
68 L. Kong, Z. Zhang, Y. Zhang, S. Liu, G. Li and X. Gao, *ACS Appl. Mater. Interfaces*, 2016, **8**, 31684–31694.
69 Y. Yang, W. Sun, J. Zhang, X. Yue, Z. Wang and K. Sun, *Electrochim. Acta*, 2016, **209**, 691–699.
70 M. K. Liu, Z. B. Yang, H. Sun, C. Lai, X. S. Zhao, H. S. Peng and T. X. Liu, *Nano Res.*, 2016, **9**, 3735–3746.
71 Y. Qiu, W. Li, W. Zhao, G. Li, Y. Hou, M. Liu, L. Zhou, F. Ye, H. Li, Z. Wei, S. Yang, W. Duan, Y. Ye, J. Guo and Y. Zhang, *Nano Lett.*, 2014, **14**, 4821–4827.
72 J. Song, T. Xu, M. L. Gordin, P. Zhu, D. Lv, Y. Jiang, Y. Chen, Y. Duan and D. Wang, *Adv. Funct. Mater.*, 2014, **24**, 1243–1250.
73 G. Zhou, E. Paek, G. S. Hwang and A. Manthiram, *Nat. Commun.*, 2015, **6**, 7760.
74 J. Song, M. L. Gordin, T. Xu, S. Chen, Z. Yu, H. Sohn, J. Lu, Y. Ren, Y. Duan and D. Wang, *Angew. Chem., Int. Ed.*, 2015, **54**, 4325–4329.
75 Z. Cao, J. Zhang, Y. Ding, Y. Li, M. Shi, H. Yue, Y. Qiao, Y. Yin and S. Yang, *J. Mater. Chem. A*, 2016, **4**, 8636–8644.
76 A. Vizintin, M. Lozinšek, R. K. Chellappan, D. Foix, A. Krajnc, G. Mali, G. Drazic, B. Genorio, R. Dedryvère and R. Dominko, *Chem. Mater.*, 2015, **27**, 7070–7081.
77 L. Y. Chai, J. X. Wang, H. Y. Wang, L. Y. Zhang, W. T. Yu and L. Q. Mai, *Nano Energy*, 2015, **17**, 224–232.
78 Q. Pang, J. Tang, H. Huang, X. Liang, C. Hart, K. C. Tam and L. F. Nazar, *Adv. Mater.*, 2015, **27**, 6021–6028.
79 J. Yang, F. Chen, C. Li, T. Bai, B. Long and X. Y. Zhou, *J. Mater. Chem. A*, 2016, **4**, 14324–14333.
80 L. Wang, Z. Yang, H. Nie, C. Gu, W. Hua, X. Xu, X. Chen, Y. Chen and S. M. Huang, *J. Mater. Chem. A*, 2016, **4**, 15343–15352.
81 L. Xing, K. Xi, Q. Li, Z. Su, C. Lai, X. Zhao and R. V. Kumar, *J. Power Sources*, 2016, **303**, 22–28.
82 X. Liang, C. Hart, Q. Pang, A. Garsuch, T. Weiss and L. F. Nazar, *Nat. Commun.*, 2015, **6**, 5682.
83 X. Liang, C. Y. Kwok, F. Lodi-Marzano, Q. Pang, M. Cuisinier, H. Huang, C. J. Hart, D. Houtarde, K. Kaup,

H. Sommer, T. Brezesinski, J. Janek and L. F. Nazar, *Adv. Energy Mater.*, 2016, **6**, 1501636.
84 W. S. Zhi, W. Li, J. J. Cha, G. Zheng, Y. Yang, M. T. McDowell, P. Hsu and Y. Cui, *Nat. Commun.*, 2013, **4**, 1331.
85 X. Tao, J. Wang, Z. Ying, Q. Cai, G. Zheng, Y. Gan, H. Huang, Y. Xia, C. Liang, W. Zhang and Y. Cui, *Nano Lett.*, 2014, **14**, 5288–5294.
86 X. Wang, G. Li, J. Li, Y. Zhang, A. Wook, A. Yu and Z. Chen, *Energy Environ. Sci.*, 2016, **9**, 2533–2538.
87 J. Huang, B. Zhang, Z. Xu, S. Abouali, M. Akbari Garakani, J. Huang and J. Kim, *J. Power Sources*, 2015, **285**, 43–50.
88 Z. B. Xiao, Z. Yang, L. Wang, H. Nie, M. Zhong, Q. Lai, X. Xu, L. J. Zhang and S. M. Huang, *Adv. Mater.*, 2015, **27**, 2891–2898.
89 G. Xu, J. Yuan, X. Tao, B. Ding, H. Dou, X. Yan, Y. Xiao and X. Zhang, *Nano Res.*, 2015, **8**, 3066–3074.
90 G. Liang, J. Wu, X. Qin, M. Liu, Q. Li, Y. He, J. Kim, B. H. Li and F. Y. Kang, *ACS Appl. Mater. Interfaces*, 2016, **8**, 23105–23113.
91 C. Y. Fan, S. Liu, H. Li, H. Wang, H. Wang, X. L. Wu, H. Z. Sun and J. P. Zhang, *ACS Appl. Mater. Interfaces*, 2016, **8**, 28689–28699.
92 C. Fan, S. Liu, H. Li, Y. Shi, H. Wang, H. Wang, H. Sun, X. Wu and J. Zhang, *J. Mater. Chem. A*, 2017, **5**, 11255–11262.
93 M. Liu, Q. Li, X. Qin, G. Liang, W. Han, D. Zhou, Y. He, B. H. Li and F. Y. Kang, *Small*, 2017, **13**, 1602539.
94 W. Kong, L. Yan, Y. Luo, D. Wang, K. Jiang, Q. Li, S. Fan and J. Wang, *Adv. Funct. Mater.*, 2017, **27**, 1606663.
95 Y. Guo, G. Zhao, N. Wu, Y. Zhang, M. Xiang, B. Wang, H. Liu and H. Wu, *ACS Appl. Mater. Interfaces*, 2016, **8**, 34185–34193.
96 W. Sun, X. Ou, X. Yue, Y. Yang, Z. Wang, D. Rooney and K. Sun, *Electrochim. Acta*, 2016, **207**, 198–206.
97 Z. Ma, Z. Li, K. Hu, D. Liu, J. Huo and S. Wang, *J. Power Sources*, 2016, **325**, 71–78.
98 J. Park, B. Yu, J. S. Park, J. W. Choi, C. Kim, Y. Sung and J. B. Goodenough, *Adv. Energy Mater.*, 2017, **7**, 1602567.
99 G. Zhou, Y. Zhao, C. Zu and A. Manthiram, *Nano Energy*, 2015, **12**, 240–249.
100 L. Yang, G. Li, X. Jiang, T. Zhang, H. Lin and J. Y. Lee, *J. Mater. Chem. A*, 2017, **5**, 12506–12512.
101 Z. Liang, G. Zheng, W. Li, Z. W. Seh, H. Yao, K. Yan, D. Kong and Y. Cui, *ACS Nano*, 2014, **8**, 5249–5256.
102 T. H. Zhou, W. Lv, J. Li, G. M. Zhou, Y. Zhao, S. X. Fan, B. Liu, B. H. Li, F. Y. Kang and Q. H. Yang, *Energy Environ. Sci.*, 2017, **10**, 1694–1703.
103 Q. Zhang, Y. Wang, Z. W. Seh, Z. Fu, R. Zhang and Y. Cui, *Nano Lett.*, 2015, **15**, 3780–3786.
104 X. Zhang, K. Wang, X. Wei and J. Chen, *Chem. Mater.*, 2011, **23**, 5290–5292.
105 Z. Yuan, H. Peng, T. Hou, J. Huang, C. Chen, D. Wang, X. Cheng, F. Wei and Q. Zhang, *Nano Lett.*, 2016, **16**, 519–527.
106 H. G. Fuchtbauer, A. K. Tuxen, P. G. Moses, H. Topsoe, F. Besenbacher and J. V. Lauritsen, *Phys. Chem. Chem. Phys.*, 2013, **15**, 15971–15980.
107 Y. Fan, Z. Yang, W. Hua, D. Liu, T. Tao, M. M. Rahman, W. Lei, S. Huang and Y. Chen, *Adv. Energy Mater.*, 2017, **7**, 1602380.
108 W. Li, Q. Zhang, G. Zheng, Z. W. Seh, H. Yao and Y. Cui, *Nano Lett.*, 2013, **13**, 5534–5540.
109 Y. M. Cui, Z. Y. Wen, X. Liang, Y. Lu, J. Jin, M. F. Wu and X. W. Wu, *Energy Environ. Sci.*, 2012, **5**, 7893–7897.
110 G. Ma, Z. Wen, J. Jin, M. Wu, X. Wu and J. Zhang, *J. Power Sources*, 2014, **267**, 542–546.
111 G. Ma, Z. Wen, Q. Wang, C. Shen, P. Peng, J. Jin and X. Wu, *J. Power Sources*, 2015, **273**, 511–516.
112 Y. S. Zhu, S. Y. Xiao, Y. Shi, Y. Q. Yang, Y. Y. Hou and Y. P. Wu, *Adv. Energy Mater.*, 2014, **4**, 1300647.
113 N. Yan, X. Yang, W. Zhou, H. Zhang, X. Li and H. Zhang, *RSC Adv.*, 2015, **5**, 26273–26280.
114 Z. Wang, J. Zhang, Y. Yang, X. Yue, X. Hao, W. Sun, D. Rooney and K. Sun, *J. Power Sources*, 2016, **329**, 305–313.
115 Q. Li, M. Liu, X. Qin, J. Wu, W. Han, G. Liang, D. Zhou, Y. He, B. H. Li and F. Y. Kang, *J. Mater. Chem. A*, 2016, **4**, 12973–12980.
116 Y. Y. Xiang, J. S. Li, J. H. Lei, D. Liu, Z. Z. Xie, D. Y. Qu, K. Li, T. F. Deng and H. L. Tang, *ChemSusChem*, 2016, **9**, 3023–3039.
117 N. Deng, W. Kang, Y. Liu, J. Ju, D. Wu, L. Li, B. S. Hassan and B. Cheng, *J. Power Sources*, 2016, **331**, 132–155.
118 Y. E. Miao, G. N. Zhu, H. Q. Hou, Y. Y. Xia and T. X. Liu, *J. Power Sources*, 2013, **226**, 82–86.
119 J. Sun, Y. Sun, M. Pasta, G. Zhou, Y. Li, W. Liu, F. Xiong and Y. Cui, *Adv. Mater.*, 2016, **28**, 9797–9803.
120 J. Huang, Q. Zhang and F. Wei, *Energy Storage Mater.*, 2015, **1**, 127–145.
121 S. Chung and A. Manthiram, *Adv. Funct. Mater.*, 2014, **24**, 5299–5306.
122 S. Chung and A. Manthiram, *J. Phys. Chem. Lett.*, 2014, **5**, 1978–1983.
123 Z. Zhang, G. Wang, Y. Lai, J. Li, Z. Zhang and W. Chen, *J. Power Sources*, 2015, **300**, 157–163.
124 J. Balach, T. Jaumann, M. Klose, S. Oswald, J. Eckert and L. Giebeler, *Adv. Funct. Mater.*, 2015, **25**, 5285–5291.
125 U. Stoeck, J. Balach, M. Klose, D. Wadewitz, E. Ahrens, J. Eckert and L. Giebeler, *J. Power Sources*, 2016, **309**, 76–81.
126 F. Zeng, Z. Jin, K. Yuan, S. Liu, X. Cheng, A. Wang, W. Wang and Y. Yang, *J. Mater. Chem. A*, 2016, **4**, 12319–12327.
127 N. Q. Liu, B. C. Huang, W. K. Wang, H. Y. Shao, C. M. Li, H. Zhang, A. B. Wang, K. G. Yuan and Y. Q. Huang, *ACS Appl. Mater. Interfaces*, 2016, **8**, 16101–16107.
128 L. Fan, H. L. Zhuang, K. Zhang, V. R. Cooper, Q. Li and Y. Y. Lu, *Adv. Sci.*, 2016, **3**, 1600175.
129 C. Chang, S. Chung and A. Manthiram, *Small*, 2016, **12**, 174–179.
130 J. Zhu, Y. Ge, D. Kim, Y. Lu, C. Chen, M. Jiang and X. Zhang, *Nano Energy*, 2016, **20**, 176–184.
131 Y. Jiang, F. Chen, Y. Gao, Y. Wang, S. Wang, Q. Gao, Z. Jiao, B. Zhao and Z. Chen, *J. Power Sources*, 2017, **342**, 929–938.
132 X. Yuan, L. Wu, X. He, K. Zeinu, L. Huang, X. Zhu, H. Hou, B. Liu, J. Hu and J. Yang, *Chem. Eng. J.*, 2017, **320**, 178–188.

133 H. Peng, D. Wang, J. Huang, X. Cheng, Z. Yuan, F. Wei and Q. Zhang, *Adv. Sci.*, 2016, **3**, 1500268.
134 Y. B. Zhang, L. Miao, J. Ning, Z. Xiao, L. Hao, B. Wang and L. J. Zhi, *2D Mater.*, 2015, **2**, 024013.
135 Z. Zhang, Y. Lai, Z. Zhang, K. Zhang and J. Li, *Electrochim. Acta*, 2014, **129**, 55–61.
136 H. Yao, K. Yan, W. Li, G. Zheng, D. Kong, Z. W. Seh, V. K. Narasimhan, Z. Liang and Y. Cui, *Energy Environ. Sci.*, 2014, **7**, 3381–3390.
137 J. Balach, T. Jaumann, S. Muehlenhoff, J. Eckert and L. Giebeler, *Chem. Commun.*, 2016, **52**, 8134–8137.
138 S. Y. Bai, X. Z. Liu, K. Zhu, S. C. Wu and H. S. Zhou, *Nat. Energy*, 2016, **1**, 16094.
139 T. Yim, S. H. Han, N. H. Park, M. Park, J. H. Lee, J. Shin, J. W. Choi, Y. Jung, Y. N. Jo, J. Yu and K. J. Kim, *Adv. Funct. Mater.*, 2016, **26**, 7817–7823.
140 Z. A. Ghazi, X. He, A. M. Khattak, N. A. Khan, B. Liang, A. Iqbal, J. Wang, H. Sin, L. Li and Z. Tang, *Adv. Mater.*, 2017, **29**, 1606817.
141 J. Li, Y. Huang, S. Zhang, W. Jia, X. Wang, Y. Guo, D. Jia and L. Wang, *ACS Appl. Mater. Interfaces*, 2017, **9**, 7499–7504.
142 Y. Zhao, M. Liu, W. Lv, Y. B. He, C. Wang, Q. B. Yun, B. H. Li, F. Y. Kang and Q. H. Yang, *Nano Energy*, 2016, **30**, 1–8.
143 J. Song, D. Su, X. Xie, X. Guo, W. Bao, G. Shao and G. Wang, *ACS Appl. Mater. Interfaces*, 2016, **8**, 29427–29433.
144 C. Lin, W. Zhang, L. Wang, Z. Wang, W. Zhao, W. Duan, Z. Zhao, B. Liu and J. Jin, *J. Mater. Chem. A*, 2016, **4**, 5993–5998.
145 J. Zhu, E. Yildirim, K. Aly, J. Shen, C. Chen, Y. Lu, M. Jiang, D. Kim, A. E. Tonelli, M. A. Pasquinelli, P. D. Bradford and X. Zhang, *J. Mater. Chem. A*, 2016, **4**, 13572–13581.
146 S. Bai, K. Zhu, S. Wu, Y. Wang, J. Yi, M. Ishida and H. Zhou, *J. Mater. Chem. A*, 2016, **4**, 16812–16817.
147 J. Q. Huang, Q. Zhang, H. J. Peng, X. Y. Liu, W. Z. Qian and F. Wei, *Energy Environ. Sci.*, 2014, **7**, 347–353.
148 G. C. Li, H. K. Jing, Z. Su, C. Lai, L. Chen, C. C. Yuan, H. H. Li and L. Liu, *J. Mater. Chem. A*, 2015, **3**, 11014–11020.
149 G. Ma, F. Huang, Z. Wen, Q. Wang, X. Hong, J. Jin and X. Wu, *J. Mater. Chem. A*, 2016, **4**, 16968–16974.
150 I. Bauer, S. Thieme, J. Brückner, H. Althues and S. Kaskel, *J. Power Sources*, 2014, **251**, 417–422.
151 J. Conder, A. Forner-Cuenca, E. M. Gubler, L. Gubler, P. Novák and S. Trabesinger, *ACS Appl. Mater. Interfaces*, 2016, **8**, 18822–18831.
152 P. Zhai, H. Peng, X. Cheng, L. Zhu, J. Huang, W. Zhu and Q. Zhang, *Energy Storage Mater.*, 2017, **7**, 56–63.
153 S. Chung and A. Manthiram, *Adv. Mater.*, 2014, **26**, 7352–7357.
154 G. Wang, Y. Lai, Z. Zhang, J. Li and Z. Zhang, *J. Mater. Chem. A*, 2015, **3**, 7139–7144.
155 H. Wei, J. Ma, B. Li, Y. Zuo and D. Xia, *ACS Appl. Mater. Interfaces*, 2014, **6**, 20276–20281.
156 C. Chang, S. Chung and A. Manthiram, *J. Mater. Chem. A*, 2015, **3**, 18829–18834.
157 T. Zhuang, J. Huang, H. Peng, L. He, X. Cheng, C. Chen and Q. Zhang, *Small*, 2016, **12**, 381–389.
158 Q. Xu, G. C. Hu, H. L. Bi and H. F. Xiang, *Ionics*, 2015, **21**, 981–986.
159 H. Peng, Z. Zhang, J. Huang, G. Zhang, J. Xie, W. Xu, J. Shi, X. Chen, X. Cheng and Q. Zhang, *Adv. Mater.*, 2016, **28**, 9551–9558.
160 Z. Q. Jin, K. Xie, X. B. Hong, Z. Q. Hu and X. Liu, *J. Power Sources*, 2012, **218**, 163–167.
161 X. Yu, J. Joseph and A. Manthiram, *J. Mater. Chem. A*, 2015, **3**, 15683–15691.
162 J. Zhu, C. Chen, Y. Lu, J. Zang, M. Jiang, D. Kim and X. Zhang, *Carbon*, 2016, **101**, 272–280.
163 L. N. Wang, J. Y. Liu, S. Haller, Y. G. Wang and Y. Y. Xia, *Chem. Commun.*, 2015, **51**, 6996–6999.
164 J. Zhu, M. Yanilmaz, K. Fu, C. Chen, Y. Lu, Y. Ge, D. Kim and X. Zhang, *J. Membr. Sci.*, 2016, **504**, 89–96.
165 J. Zhu, Y. Ge, D. Kim, Y. Lu, C. Chen, M. Jiang and X. Zhang, *Nano Energy*, 2016, **20**, 176–184.
166 L. Wang, Y. Zhao, M. L. Thomas, A. Dutta and H. R. Byon, *ChemElectroChem*, 2016, **3**, 152–157.
167 Q. S. Wang, Z. Y. Wen, J. Jin, J. Guo, X. Huang, J. H. Yang and C. H. Chen, *Chem. Commun.*, 2016, **52**, 1637–1640.
168 Q. F. Wang, *Electrochim. Acta*, 2015, **182**, 334–341.
169 C. Fan, H. Yuan, H. Li, H. Wang, W. Li, H. Sun, X. Wu and J. Zhang, *ACS Appl. Mater. Interfaces*, 2016, **8**, 16108–16115.
170 C. Lin, W. K. Zhang, L. Wang, Z. G. Wang, W. Zhao, W. H. Duan, Z. G. Zhao, B. Liu and J. Jin, *J. Mater. Chem. A*, 2016, **4**, 5993–5998.
171 S. Evers and L. F. Nazar, *Acc. Chem. Res.*, 2013, **46**, 1135–1143.
172 G. Zhou, S. Pei, L. Li, D. Wang, S. Wang, K. Huang, L. Yin, F. Li and H. M. Cheng, *Adv. Mater.*, 2014, **26**, 625–631.
173 H. Q. Wang, W. C. Zhang, H. K. Liu and Z. P. Guo, *Angew. Chem., Int. Ed.*, 2016, **55**, 3992–3996.
174 G. M. Zhou, L. Li, D. W. Wang, X. Y. Shan, S. F. Pei, F. Li and H. M. Cheng, *Adv. Mater.*, 2015, **27**, 641–647.
175 M. Yu, J. Ma, M. Xie, H. Song, F. Tian, S. Xu, Y. Zhou, B. Li, D. Wu, H. Qiu and R. Wang, *Adv. Energy Mater.*, 2017, **7**, 1602347.

